

Discrete signature tensors for persistence landscapes

VINCENZO GALGANO, HEATHER A. HARRINGTON, DANIEL TOLOSA

Abstract

Signature tensors of paths are a versatile tool for data analysis and machine learning. Recently, they have been applied to persistent homology, by embedding barcodes into spaces of paths. Among the different path embeddings, the persistence landscape embedding is injective and stable, however it loses injectivity when composed with the signature map. Here we address this by proposing a discrete alternative. The critical points of a persistence landscape form a time-series, of which we compute the discrete signature. We call this association the *discrete landscape feature map* (DLFM). We give results on the injectivity, stability and computability of the DLFM. We apply it to a knotted protein dataset, capturing sequence similarity and knot depth with statistical significance.

Keywords: persistent homology, barcodes, persistence landscapes, feature maps, time-series, time warping, path signatures, tensors, knotted proteins, vectorisation.

MSC2020 codes: 55N31, 68T09, 46B85.

Acknowledgements. We thank Agnese Barbensi, Darrick Lee, Vidit Nanda and Leon Renkin for helpful discussions. We also thank MPI-MiS Leipzig for hosting the conference “MEGA 2024”, which informed this research and led to new connections with Francesco Galuppi and Pierpaola Santarsiero. We are grateful to MPI-CBG Dresden and CSBD for the excellent working conditions. HAH gratefully acknowledges funding from the Royal Society RGF/EA/201074, UF150238 and EPSRC EP/R018472/1, EP/Y028872/1 and EP/Z531224/1. VG is member of the Italian national group GNSAGA-INdAM.

Open Access policy. The authors have applied a CC-BY public copyright license to any Author Accepted Manuscript (AAM) version arising from this submission.

Introduction

As the scale and complexity of biological data increases, problems such as interpretation, classification and quantification require advanced mathematical methods for investigation. Applying persistent homology from topological data analysis to biological data provides a geometric interpretation of the shapes of data. Here, we propose an alternative approach combining persistent homology and nonlinear algebra.

Persistent homology provides a multiscale geometric descriptor of data that is functorial, stable to perturbations and interpretable: it takes in a filtered simplicial complex that describes the shape of data, and then outputs a persistence module that can be visualised as a *barcode*, i.e. a multiset of intervals. Persistent homology has been applied to complex datasets (e.g. neuroscience and biomedicine [Gar+22; Lee+17; Mil15; Ben+24; RB19]). In addition to its stability and interpretability, vectorising barcodes is crucial for machine learning integration [Ali+23]. Some approaches consist of studying the analytical and topological properties of certain continuous paths (e.g. landscape embedding, integrated landscape embedding, Betti curves) associated to landscapes (or barcodes) [Bub+20; CNO20; Giu+25]. For instance, unlike Betti curves, the (integrated) landscape embedding has been proven to be stable and more meaningful, but still computationally inefficient.

In [CNO20] the authors proposed a new approach to vectorisation in topological data analysis, leading to *feature maps* which associate barcodes to the signature tensors of the aforementioned paths. More precisely, a feature map Φ_\bullet .

$$\Phi_\bullet : \mathbf{Bar} \xrightarrow{\iota_\bullet} \mathbf{BV}(V) \xrightarrow{\sigma} \mathbb{T}((V))$$

is given by the composition of a chosen *path embedding* $\iota_\bullet : \mathbf{Bar} \rightarrow \mathbf{BV}(V)$ from barcodes to bounded-variation paths, with the *Chen signature map* $\sigma : \mathbf{BV}(V) \rightarrow \mathbb{T}((V))$ associating to a path its signature tensor. *Signature tensors* are an algebraic tool firstly introduced by [Che54] with a rich algebraic and combinatorial structure based on Hopf algebras. A more geometrical approach to signature tensors was firstly proposed in [AFS19], focusing on related algebraic varieties. Since then, the topic has increasingly attracted the interest of algebraic geometers [Amé+25; GS24]. A discrete version of signature tensors was introduced by [DET20a; DET20b], called *discrete signature tensor* (or also iterated sum signature in opposition to Chen’s iterated integral signature). It associates tensors to time-series, and its combinatorics is ruled by quasi-Hopf algebras. First results on the geometry of discrete signature tensors appear in [BP23].

Our work is inspired by both feature maps from persistent homology and the discrete signature tensors. Among the feature maps proposed in [CNO20] the *landscape* and *integrated landscape* path embeddings satisfy desirable stability properties. We take a closer look at these two feature maps and at their images in $\mathbb{T}((V))$. In particular, we focus on the varieties of signature matrices of (integrated) landscape paths. However, the description we give is only partial, and intended more as invitation to algebraic geometers for further study. For instance, since persistence landscape paths are piecewise linear loops, we first describe the signature matrices for loops.

Proposition (cf. Prop. 2.1, Cor. 2.2). *A piecewise linear path is a loop if and only if its signature matrix coincides with its log-signature matrix. In particular, the variety of signature matrices of piecewise linear loops in \mathbb{R}^d with m maximal segments coincides with the secant variety $\sigma_{\lfloor \frac{m}{2} \rfloor}(Gr(2, d))$ of the Grassmannian of planes in \mathbb{R}^d .*

The main theoretical contribution of this work is a discrete approach to feature maps as an alternative for vectorisation. We introduce the *discrete landscape feature*

map (DLFM)

$$\begin{array}{ccccccc} \Phi_I : \mathbf{Bar} & \xrightarrow{\iota_{LS}} & \mathbf{BV}(V) & \rightarrow & \mathbf{TS}(V) & \xrightarrow{\Sigma} & \mathbb{T}((\mathcal{V})) \\ B & \mapsto & \lambda^B & \mapsto & \underline{\mathbf{x}}^B & \mapsto & \Sigma(\underline{\mathbf{x}}^B) \end{array}$$

which first associates to a barcode $B \in \mathbf{Bar}$ the time-series $\underline{\mathbf{x}}^B = \{\mathbf{x}_1, \dots, \mathbf{x}_n\} \in \mathbf{TS}(V)$ of critical points of the persistence landscape $\lambda^B \in \mathbf{BV}(V)$ of the barcode, and then the discrete signature tensor $\Sigma(\underline{\mathbf{x}}^B) \in \mathbb{T}((\mathcal{V}))$ of the time-series (cf. Sec. 3 for precise definitions). The map $\mathbf{BV}(V) \rightarrow \mathbf{TS}(V)$ restricted to persistence landscapes is “canonical”, since persistence landscapes are completely determined by their critical points. Of course, this method may generalise to other path embeddings.

We choose the landscape embedding and the discrete signature due to their *stability* properties and their *discriminative* powers. Indeed, the landscape embedding ι_{LS} is stable, unlike other embeddings, and injective (cf. [CNO20, Sec. 3.4]). However, the discriminative power of ι_{LS} gets lost in the feature map Φ_{LS} , since Chen signature tensors are invariant under tree-like equivalence of paths. We address this by taking a discrete approach, given the discrete nature of the output of persistent homology, and the availability of the software FRUITS (Feature Extraction Using Iterated Sums) proposed in [DK24] for efficiently implementing discrete signatures. We show that discrete signature tensors distinguish among tree-like equivalent landscapes, implying that the DLFM Φ_I is more descriptive than Φ_{LS} . Alternatively, one may solve the non-injectivity of Φ_{LS} by adding a time parameter to ι_{LS} , but we expect this would have computational limitations.

We start our analysis of the discrete feature map Φ_I by first studying the injectivity of the discrete signature map $\Sigma : \mathbf{TS}(V) \rightarrow \mathbb{T}((\mathcal{V}))$. Such a map is a monoid homomorphism with respect to the shifted-concatenation (cf. equation (3.9)) of time-series, and the tensor product of discrete signature tensors. The discrete signature map is known [DET20b] to be invariant under time-warping and time-translation equivalence \sim_{twt} . We prove that this equivalence uniquely determines the (monoidal) kernel of Σ .

Theorem (cf. Theorem 3.4). *Any two time-series $\underline{\mathbf{x}}, \underline{\mathbf{y}} \in \mathbf{TS}(V)$ have the same discrete signature $\Sigma(\underline{\mathbf{x}}) = \Sigma(\underline{\mathbf{y}})$ if and only if $\underline{\mathbf{x}} \sim_{twt} \underline{\mathbf{y}}$. In particular, the quotient map $\mathbf{TS}(V)/\sim_{twt} \hookrightarrow \mathbb{T}((\mathcal{V}))$ is injective.*

We also propose a description of time-warping and time-translation in terms of matrices (cf. Remark 3.1).

Next, we address the problem of the stability of the discrete feature map Φ_I . We note that it is not continuous on the whole domain \mathbf{Bar} , since the discrete signature map is not invariant under time-series refinements. We overcome this obstacle by restricting to consider a finite set of barcodes $D \subset \mathbf{Bar}$, and consider the union of the critical points of all landscapes arising from D . This results in the *specialised discrete landscape feature map* Φ_{I_D} . Such an assumption is reasonable considering that most experiments generate finite datasets. Moreover, we restrict the image of Φ_{I_D} to the subspace $\mathbb{T}^{\leq k}((\mathcal{V}))$ of discrete signature tensors truncated up to weight k . Again, this restriction is quite natural for applications.

The feature map Φ_{I_D} has desirable continuity properties. Indeed, albeit not being stable in the sense of 1-Lipschitz, we show that Φ_{I_D} is uniformly continuous. Here, the metrics involved are the *bottleneck distance* on the space of barcodes \mathbf{Bar} (introduced by [CEH07] and further investigated by [Bub15]) and the *Bombieri-Weyl distance* on the space of discrete signature tensors $\mathbb{T}((\mathcal{V}))$, naturally induced from the standard scalar product on $\mathbb{R}^d \simeq V$.

Theorem (cf. Theorem 3.15). *Given $D \subset \mathbf{Bar}$ a finite set of barcodes, the specialised discrete landscape feature map*

$$\Phi_{I_D}^{\leq k} : \mathbf{Bar} \rightarrow \mathbb{T}^{\leq k}((\mathcal{V}))$$

is uniformly continuous with respect to the bottleneck distance on \mathbf{Bar} and the Bombieri-Weyl distance on $\mathbb{T}^{\leq k}((\mathcal{V}))$.

We complement the theoretical study by showcasing the DLFM on a knotted protein dataset previously analysed with persistence landscapes in [Ben+23]. We use the software FRUITS (Feature Extraction Using Iterated Sums) proposed in [DK24] for implementing discrete signatures. We show that discrete signatures and structure representative classes (in the sense of amino-acid sequence similarity) are strongly correlated with very high *Adjusted Rand Index* (ARI) and *Normalised Mutual Information* (NMI) scores. We validate the statistical significance of such correlation by running permutation tests. We also show correlation between discrete signature and knot depth via two statistical methods, and we visualise it by applying Principal Component Analysis (PCA). In our analysis we maintain the labeling of representatives analogous to the one in [Ben+23] to allow comparisons. We explain our analysis in a way intended to be accessible to a broad audience.

This work is organised as follows. Sec. 1 contains the preliminary notions and already known results about signature tensors and persistence feature maps. In Sec. 2 we give partial descriptions of the signature matrices of piecewise linear loops, landscapes and integrated landscapes. Sec. 3 represents the theoretical core of the manuscript, and contains all constructions and results about the discrete landscape feature map. Sec. 4 highlights the utility of the signature-based analysis of biological structures of knotted proteins with respect to both sequence similarity and knot depth.

1 Preliminaries

1.1 Signature tensors and their varieties

Our main references for notions and result appearing in the following are [AFS19; Amé+25]. We fix a vector space V over \mathbb{R} of dimension d and a basis (e_1, \dots, e_d) .

Power series tensor algebra. Given a vector space V , let $\mathbb{T}((V)) := \prod_{k \geq 0} V^{\otimes k}$ be the *power series tensor algebra* over V , whose elements are sequences of tensors $\mathcal{T} = (T^{(k)})_k$ such that $T^{(k)} \in V^{\otimes k}$, and whose inner product is given by the tensor product $\mathcal{T} \otimes \mathcal{T}' = (\sum_{i+j=k} T^{(i)} \otimes (T')^{(j)})_k$. Equivalently, by looking at elements as power series $\mathcal{T} = \sum_{k \geq 0} T^{(k)}$, the inner product is the multiplication of power series. For any k we write $T_{i_1, \dots, i_k}^{(k)} \in \mathbb{C}$ for the (i_1, \dots, i_k) -th entry of the tensor $T^{(k)}$ with respect to the fixed basis of V , so that $T^{(k)} = \sum_{I \in [n]^k} T_{i_1, \dots, i_k}^{(k)} e_{i_1} \otimes \dots \otimes e_{i_k}$. We denote the multiplicative subgroup of $\mathbb{T}((V))$ of power series with degree-0 term equal to 1 by

$$\mathbb{T}_1((V)) := \{\mathcal{T} \in \mathbb{T}((V)) \mid T^{(0)} = 1\}.$$

Path signature. Let $\mathbf{BV}([0, 1], V)$ be the set of bounded-variation continuous paths $\gamma : [0, 1] \rightarrow V$. The *path signature* is the map

$$\begin{aligned} \sigma : \mathbf{BV}([0, 1], V) &\longrightarrow \mathbb{T}_1((V)) \\ \gamma &\mapsto \sigma(\gamma) = (\sigma^{(k)}(\gamma))_k \end{aligned} \quad (1.1)$$

such that $\sigma^{(0)}(\gamma) = 1$ by convention, and $\sigma^{(k)}(\gamma) := \int_{\Delta_k} d\gamma^{\otimes k}$ is the Riemann-Stieltjes integral of $d\gamma^{\otimes k} := d\gamma(t_1) \otimes \dots \otimes d\gamma(t_k)$ over the k -dimensional standard simplex Δ_k . More practically, the coefficient of $e_{i_1} \otimes \dots \otimes e_{i_k}$ in the tensor $\sigma^{(k)}(\gamma) \in V^{\otimes k}$ is (cf. [Che54, Secc. 2, 3])

$$\sigma^{(k)}(\gamma)_{i_1, \dots, i_k} = \int_0^1 \int_0^{t_1} \dots \int_0^{t_{k-1}} \dot{\gamma}_{i_1}(t_1) \dots \dot{\gamma}_{i_k}(t_k) dt_1 \dots dt_k. \quad (1.2)$$

The sequence $\sigma(\gamma) \in \mathbb{T}((V))$ is the *signature tensor* of γ , and its k -th entry $\sigma^{(k)}(\gamma) \in V^{\otimes k}$ is the *order- k signature tensor* of γ .

The path signature σ is a multiplicative homomorphism with respect to the concatenation of paths in $\mathbf{BV}([0, 1], V)$ (which we denote by $*$) and the tensor product in $\mathbb{T}_1((V))$. This is a consequence of the Chen relation [Che54, Theorem 3.1]

$$\sigma(\gamma_1 * \gamma_2) = \sigma(\gamma_1) \otimes \sigma(\gamma_2). \quad (1.3)$$

Moreover, σ quotients to an injective homomorphism

$$\sigma : \mathbf{BV}([0, 1], V) / \sim_{tl} \hookrightarrow \mathbb{T}_1((V)) \quad (1.4)$$

with respect to the *tree-like equivalence*, for whose definition we refer to [CNO20, Sec. 4]. However, [HL10, Corollary 1.5] shows that one can take $\gamma_1 \sim_{tl} \gamma_2 \iff \sigma(\gamma_1 * \gamma_2^{-1}) = (1, \mathbf{0}, \dots)$ as definition.

Remark 1.1. The name *tree-like equivalence* comes from the fact that in a tree (say, path of segments without loops) one can always iteratively retract leaves up to a point, giving a trivial signature.

Remark 1.2. The natural action of $\mathrm{GL}(V)$ on V induces an entry-wise action on each $V^{\otimes k}$, hence on $\mathbb{T}_1((V))$, as well as on $\mathbf{BV}([0, 1], V)$ where $(g \cdot \gamma)(t) = g \cdot (\gamma(t))$. In particular, the path signature map σ is $\mathrm{GL}(V)$ -equivariant, that is $g \cdot \sigma(\gamma) = \sigma(g \cdot \gamma)$. Finally, signatures are invariant under translations and reparametrisations of paths. We will therefore always consider paths based at the origin, i.e. $\gamma(0) = \mathbf{0} \in V$.

Varieties of signature matrices. From the point of view of algebraic geometry, it is standard and often convenient to work over \mathbb{C} and therefore consider the signature tensors as elements in the complexification of $\mathbb{T}((V))$, for which we use the same notation. We are interested in algebro-geometric relations among signature tensors, which naturally lead us to study algebraic varieties defined by the path signature map. For any $k \geq 1$, consider the composition of the path signature with the projection of the tensor algebra on its k -th graded component

$$\begin{aligned} \sigma^{(k)} : \mathbf{BV}([0, L], V) &\longrightarrow V^{\otimes k} \\ \gamma &\mapsto \sigma^{(k)}(\gamma) \end{aligned}$$

assigning to each path its order- k signature tensor. The k -th *universal signature variety* $\mathcal{U}_{d,k}$ is the Zariski closure of the (projectivisation) of the image of $\sigma^{(k)}$ inside $\mathbb{P}(V^{\otimes k})$ (cf. [AFS19, Sec. 4.3]).

We focus on the case $k = 2$, namely *varieties of signature matrices*. By construction, these lie in the universal signature varieties $\mathcal{U}_{d,2}$. Given $\gamma \in \mathbf{BV}([0, L], V)$, from (1.2) one has that $\sigma^{(2)}(\gamma) \in \mathbb{R}^{d \times d}$ is a matrix whose ij entry is

$$\sigma_{ij}^{(2)}(\gamma) = \int_0^L \gamma_i(s) \dot{\gamma}_j(s) ds. \quad (1.5)$$

We denote the symmetric and skew-symmetric part of $\sigma^{(2)}$ by $\sigma_{\text{sym}}^{(2)} := \frac{1}{2}(\sigma^{(2)} + (\sigma^{(2)})^{\mathbf{T}})$ and $\sigma_{\text{skew}}^{(2)} := \frac{1}{2}(\sigma^{(2)} - (\sigma^{(2)})^{\mathbf{T}})$ respectively. Applying integration by parts to (1.5) leads to

$$2\sigma_{\text{sym}}^{(2)} = \gamma(L)^{\otimes 2}. \quad (1.6)$$

In fact, signature matrices are precisely those matrices with rank-1 symmetric part [AFS19, Secc. 2, 3], that is

$$\mathcal{U}_{d,2} = \left\{ v \otimes v + Q \mid v \in V, Q \in \bigwedge^2 V \right\}. \quad (1.7)$$

Signatures of PWL paths. We refer to *piecewise linear* (PWL) paths as continuous paths $\gamma : [0, L] \rightarrow V$ which are concatenation of finitely many segments $\gamma = \alpha_1 * \dots * \alpha_m$, where $\alpha_j(t) = \mathbf{a}_j \cdot t$ for certain $\mathbf{a}_j \in V$. The partition $\gamma = \alpha_1 * \dots * \alpha_m$ is unique if we require that the segments $\alpha_1, \dots, \alpha_m$ have maximal length possible, or equivalently that m is minimal.

Definition 1.3. We refer to such partition as the *minimal segment decomposition* (MSD) of the path, and we say that the path γ is m -piecewise linear (m -PWL).

Signatures of PWL paths have a particularly nice expression in terms of their segment decomposition. The k -th signature tensor of a segment path $\alpha(t) = \mathbf{a} \cdot t$ for $\mathbf{a} \in V$ is always the symmetric rank-1 tensor determined by \mathbf{a} , that is

$$\sigma(\alpha) = \left(1, L\mathbf{a}, \frac{L^2}{2}\mathbf{a}^{\otimes 2}, \dots, \frac{L^k}{k!}\mathbf{a}^{\otimes k}, \dots \right) = \exp(L\mathbf{a}).$$

In fact, segments (up to tree-like equivalence) are the only paths with rank 1 signature. Then by Chen's relation (1.3) the signature tensor of a m -PWL path $\gamma = \alpha_1 * \dots * \alpha_m$ is

$$\sigma(\gamma) = \exp(\mathbf{a}_1) \otimes \dots \otimes \exp(\mathbf{a}_m) . \quad (1.8)$$

Let $\mathcal{M}_{d,m}$ be the variety of signature matrices of m -PWL paths in V . Then for any m

$$\mathcal{M}_{d,m} = \{v \otimes v + Q \mid v \in V, \text{rk}[v \otimes v|Q] \leq m\} , \quad (1.9)$$

where $[v \otimes v|Q]$ is the matrix obtained by attaching the rank-1 matrix $v \otimes v$ and the matrix Q . The varieties $\mathcal{M}_{d,m}$ define a filtration starting at the Veronese variety $\nu_2(\mathbb{P}^{d-1})$ and stabilizing at the universal variety of signature matrices [AFS19, Theorem 3.4, Example 4.12]

$$\nu_2(\mathbb{P}^{d-1}) = \mathcal{M}_{d,1} \subset \mathcal{M}_{d,2} \subset \dots \subset \mathcal{M}_{d,d} = \mathcal{U}_{d,2} \subset \mathbb{P}(V^{\otimes 2}) .$$

1.2 Persistence feature maps

A *barcode* is a multiset of intervals of the form $B := \{[b_1, d_1), \dots, [b_n, d_n)\}$, where $b_i \leq d_i$ are non-negative real numbers called *birth* and *death*. Barcodes, or equivalently persistence diagrams, are the standard output of persistent homology, the flagship method in topological data analysis. We refer to [Ott+17] for a basic introduction to the topic. In this paper, we will assume barcodes to be *tame*, that is they have only finitely many intervals, and all intervals are contained in a certain $[0, L]$.

From [Bub15] we recall that any barcode B defines a family of continuous functions $\lambda_k^B : \mathbb{R} \rightarrow \mathbb{R}$ such that

$$\lambda_k^B(t) := \sup\{s \geq 0 \mid \beta^{t-s, t+s} \geq k\},$$

where $\beta^{t-s, t+s}$ is the number of intervals in B that contain $[t-s, t+s]$, and where one sets $\lambda_k^B(t) = 0$ whenever the supremum is taken over the empty set (cf. [CNO20, Definition 3.2]). The function $\lambda_k^B(t)$ is called the k -th *landscape* of the barcode B [Bub20], or k -th *level* of B .

Remark 1.4. A graphical construction of the landscape of a barcode is as follows. Let B be a barcode with bars (B_1, \dots, B_n) . For any $i \in [n]$, consider the birth-death point $P_i := (a_i, b_i) \in \mathbb{R}^2$ such that B_i is supported on $[a_i, b_i]$. By definition, each birth-death point lies above the diagonal in \mathbb{R}^2 , and defines a right triangle whose hypotenuse lies on the diagonal and whose catheti meet in the point itself. After isometries of the plane, one consider all these hypotenuses lying on the interval $[0, L]$ along the x -axis. The persistence landscape of B is the union of the sides of such triangles.

By construction, levels of a landscape λ^B are PWL paths $\lambda_j^B : [0, L] \rightarrow \mathbb{R}$, such that

- they are loops: $\lambda_j^B(0) = \lambda_j^B(L) = 0$;
- higher levels dominate lower levels: $\lambda_i^B(t) \geq \lambda_j^B(t)$ for any $t \in [0, L]$ and $i \leq j$;

- for any $j \in [d]$ the segments of λ_j^B have slope in $\{0, \pm 1\}$.

We write $\lambda^B = (\lambda_1, \dots, \lambda_d)$ by non specifying B at each level when it is clear.

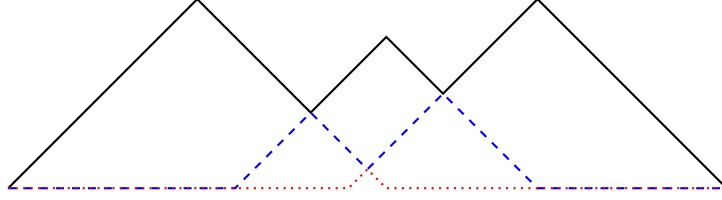


Figure 1.1: Landscape with 3 levels: λ_1 in black, λ_2 in blue, λ_3 in red.

In the need of vectorising barcodes, several ways of associating paths in a vector space to barcodes have been introduced under the name of *embeddings*. Moreover, in order to obtain a more informative vectorisation, in [CNO20] the authors composed such embeddings with the Chen signature map (1.1): an embedding $\iota_\bullet : \mathbf{Bar} \rightarrow \mathbf{BV}([0, L], \mathbb{R}^d)$ defines the *feature map*

$$\Phi_\bullet : \mathbf{Bar} \xrightarrow{\iota_\bullet} \mathbf{BV}([0, L], \mathbb{R}^d) \xrightarrow{\sigma} \mathbb{T}_1((\mathbb{R}^d)) .$$

Note that the feature map Φ_\bullet quotients to an injective map under the tree-like equivalence. In the following we focus on two feature maps, but we refer to [CNO20] for a more complete overview.

The *landscape embedding* is the map associating to each barcode B (with at most d levels) a path λ^B in \mathbb{R}^d whose k -entry is the k -th level of B , namely

$$\begin{aligned} \iota_{\text{LS}} : \mathbf{Bar} &\longrightarrow \mathbf{BV}([0, L], \mathbb{R}^d) \\ B &\mapsto \lambda^B(t) = \begin{bmatrix} \lambda_1^B(t) \\ \vdots \\ \lambda_d^B(t) \end{bmatrix} . \end{aligned} \quad (1.10)$$

Such vectorisation is not as descriptive as one would desire. The tree-like equivalence of paths makes impossible to distinguish large classes of landscapes. For example, the empty barcode, a singleton barcode $\{[b, d]\}$ and any barcode $\{[b_1, d_1), \dots, [b_n, d_n)\}$ such that $b_i > d_{i-1}$, $i = 2, \dots, n$, define tree-like paths. Hence, the feature map Φ_{LS} maps each of them to the trivial signature $(1, \mathbf{0}, \dots)$.

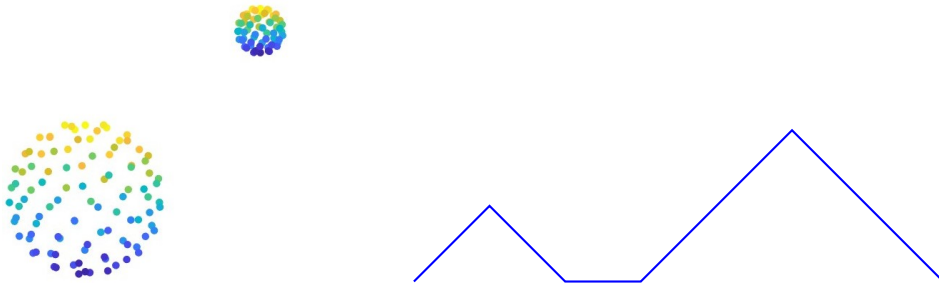


Figure 1.2: Uniform sampling, called *Fibonacci sampling*, of two spheres (left) has a one-dimensional associated persistence landscape (right) with trivial Chen signature.

A more descriptive embedding is given by a cumulative version of ι_{LS} , which distinguishes more features of barcodes at the cost of an additional integration step. The *integrated landscape embedding* is the map

$$\begin{aligned} \iota_{\text{iLS}} : \mathbf{Bar} &\longrightarrow \mathbf{BV}([0, L], \mathbb{R}^d) \\ B &\mapsto F^{\lambda^B}(t) := \begin{bmatrix} \int_0^t \lambda_1^B(s) ds \\ \vdots \\ \int_0^t \lambda_d^B(s) ds \end{bmatrix}. \end{aligned} \quad (1.11)$$

The key property of the resulting feature map Φ_{iLS} is its stability (under perturbations of the barcodes). However, the extra integration step makes it computationally inefficient.

Some initial work has been done to describe invariants of signature tensors [GS24; Amé+25] and it would be interesting to relate these invariants to the topology of barcodes via the feature maps. For instance, the only rank-1 signature tensors are signatures of segments [Amé+25, Corollary 7.3]. In the case of the landscape feature map ι_{LS} , the latter result leads to the following.

Proposition 1.5. *Given a barcode B , the signature tensor $\Phi_{\text{LS}}(B) = \sigma(\lambda^B)$ (resp. $\Phi_{\text{iLS}}(B) = F^{\lambda}$) has rank 1 —i.e. for any $k \geq 0$ the k -th signature $\sigma^{(k)}(\lambda^B)$ has tensor-rank 1 in $V^{\otimes k}$ — if and only if the barcode B is trivial —i.e. it consists of diagonal birth-death points $[a_i, a_i]$.*

2 Signature tensors of persistence landscapes

This section is devoted to partial results on the Chen signature tensors of persistence landscape paths. It would be worth investigating more the geometry of such signature tensors in order to deduce algebraic-geometric descriptions of barcodes. However, this goes beyond our current scope, and we leave it for future work.

Signature tensors of PWL loops. Since landscapes are piecewise linear (PWL) loops, it is quite natural to first describe the signature varieties of such larger class of paths. Since signature tensors are invariant under translation, we consider loops starting and ending at $\mathbf{0} \in \mathbb{R}^d$.

We show that PWL loops are characterised by a precise behaviour of their signature matrices. In the following, we denote by $\log \sigma(\lambda)$ the *log-signature* of λ , a sequence of tensors defined by the property that $\sigma(\lambda) = \exp(\log \sigma(\lambda))$, and by $\log \sigma^{(k)}(\lambda)$ its k -th entry. We refer to [FLS24] for properties of the log-signature. Note that, by definition of the exponential map, the following truncations hold:

$$\begin{aligned} \sigma^{(1)}(\lambda) &= \log \sigma^{(1)}(\lambda), \\ \sigma^{(2)}(\lambda) &= \log \sigma^{(2)}(\lambda) + \frac{1}{2} \left(\log \sigma^{(1)}(\lambda) \right)^2, \\ \sigma^{(3)}(\lambda) &= \log \sigma^{(3)}(\lambda) + \frac{1}{2} \left(\log \sigma^{(1)}(\lambda) \log \sigma^{(2)}(\lambda) + \log \sigma^{(2)}(\lambda) \log \sigma^{(1)}(\lambda) \right) + \frac{1}{6} \left(\log \sigma^{(1)}(\lambda) \right)^3. \end{aligned}$$

Each tensor space $(\mathbb{R}^d)^{\otimes k}$ admits a decomposition as direct sum in Thrall modules, for whose definition we refer to [Amé+25, Sec. 3]. Each summand in the right-hand sides of the above equations belongs to a different Thrall module, so all summands are linearly independent.

Proposition 2.1. *Let λ be a PWL path with MSD $\alpha_1 * \dots * \alpha_m$ where $\alpha_j(t) = \mathbf{a}_j t + c_j$ for $\mathbf{a}_j \in \mathbb{R}^d$ and suitable c_j in order to make the path conjunction continuous. The following facts are equivalent:*

1. λ is a loop;
2. $\sigma^{(1)}(\lambda) = \log \sigma^{(1)}(\lambda) = \mathbf{0}$;
3. $\sigma^{(2)}(\lambda) = \log \sigma^{(2)}(\lambda) = \frac{1}{2} \sum_{i < j} \mathbf{a}_i \wedge \mathbf{a}_j$;
4. $\sigma^{(3)}(\lambda) = \log \sigma^{(3)}(\lambda)$.

Proof. In the above notation, the first signature of the m -PWL path λ is $\sigma^{(1)}(\lambda) = \mathbf{a}_1 + \dots + \mathbf{a}_m$. The latter sum being the zero vector is equivalent to λ being a loop. Moreover, the first signature always coincides with the first log-signature, hence (1) \iff (2).

The second equality in (3) always holds (cf. [FLS24, Example 7.3]). If the first log-signature is zero, then $\sigma^{(2)}(\lambda) = \log \sigma^{(2)}(\lambda)$. On the contrary, if the first equality in (3) holds, then $(\log \sigma^{(1)}(\lambda))^2 = \mathbf{0}$ (as matrices) implies $\log \sigma^{(1)}(\lambda) = \mathbf{0}$ (as vectors). This proves (2) \iff (3).

Finally, the equivalence (2) \iff (4) follows from the linear independence among summands lying in different Thrall modules. \square

The above characterisations of PWL loops in terms of their signature matrices allow to describe the corresponding varieties. We denote the variety of signature matrices for m -PWL loops in \mathbb{R}^d by

$$\mathcal{M}_{d,m}^\circ := \overline{\{\sigma^{(2)}(\lambda) \mid \lambda \text{ } m\text{-PWL loop in } \mathbb{R}^d\}} \subset \mathcal{M}_{d,m} \subset \mathbb{P}(\mathbb{R}^{d \times d}) ,$$

and the variety of signature matrices of loops in \mathbb{R}^d (not necessarily PWL) by

$$\mathcal{U}_{d,2}^\circ := \overline{\{\sigma^{(2)}(\lambda) \mid \lambda \text{ loop in } \mathbb{R}^d\}} \subset \mathcal{U}_{d,2} .$$

Let $Gr(2, d)$ the Grassmannian of planes in \mathbb{R}^d , corresponding to $d \times d$ skew-symmetric matrices of rank 2, and let $\sigma_r(Gr(2, d))$ be the r -th secant variety of $Gr(2, d)$, corresponding to $d \times d$ skew-symmetric matrices of rank at most $2r$.

Corollary 2.2. *In the above notation, it holds:*

1. $\mathcal{U}_{d,2}^\circ = \mathbb{P}(\bigwedge^2 V)$;
2. $\mathcal{M}_{d,m}^\circ = \sigma_{\lfloor \frac{m}{2} \rfloor}(Gr(2, d))$, for any $m \leq d$.

In particular, $\mathcal{M}_{d,d+h}^\circ = \mathcal{U}_{d,2}^\circ = \mathbb{P}(\bigwedge^2 V)$ for any $h \geq 0$.

Proof. Up to translation, a loop $\lambda : [0, L] \rightarrow \mathbb{R}^d$ is such that $\lambda(0) = \lambda(L) = \mathbf{0}$, hence the signature matrix of λ has symmetric part $\sigma_{\text{sym}}^{(2)}(\lambda) = \frac{1}{2}(\lambda(L) - \lambda(0))^{\otimes 2} = \mathbf{0}^{\otimes 2}$. This also follows from Proposition 2.1. Then the two theses follow straightforward from the definitions (1.7) and (1.9) by cutting the varieties $\mathcal{M}_{d,m} \subset \mathcal{U}_{d,2} \subset \mathbb{P}(V^{\otimes d})$ by $\mathbb{P}(\bigwedge^d V)$. \square

Signature tensors of landscapes. By construction, the number m of segments in the MSD of a landscape with d levels (i.e. a landscape path in \mathbb{R}^d) is *strictly lower bounded* by d , that is $d \lesssim m$. Thus it makes sense to consider the (universal) variety of signature matrices of landscapes in \mathbb{R}^d regardless of the number of linear pieces in the MSD. We denote such variety by

$$\mathcal{M}_{d,2}^{\text{LS}} := \overline{\{\sigma^{(2)}(\lambda) \mid \lambda \text{ landscape path in } \mathbb{R}^d\}} \subset \mathcal{M}_{d,2}^{\circ} = \mathbb{P}\left(\bigwedge^2 \mathbb{R}^d\right).$$

Consider a landscape path $\lambda^B(t) = (\lambda_1(t), \dots, \lambda_d(t)) \subset \mathbb{R}^d$ with MSD $\lambda^B = \alpha_1 * \dots * \alpha_m$ defined on the partition $[0, t_1] \cup [t_1, t_2] \cup \dots \cup [t_{m-1}, L]$ such that each segment $\alpha_j : [t_{j-1}, t_j] \rightarrow \mathbb{R}^d$ is defined as

$$\alpha_j(t) = \mathbf{a}_j \cdot t + \alpha_{j-1}(t_{j-1})$$

for a suitable $\mathbf{a}_j = (a_{1j}, \dots, a_{dj})^T \in \{-1, 0, 1\}^d$. Then each λ^B defines a $d \times m$ matrix

$$X_\lambda := [\mathbf{a}_1 \mid \dots \mid \mathbf{a}_m].$$

The conditions on the levels of a landscape (cf. Sec. 1.2) impose some semialgebraic conditions, besides the algebraic condition of being a loop: clearly, $\mathcal{M}_{d,2}^{\text{LS}} \subseteq \mathcal{M}_{d,2}^{\circ} = \mathbb{P}(\bigwedge^2 \mathbb{R}^d)$. For instance, the non-negativity of sums over each row implies $\mathbf{a}_1 + \dots + \mathbf{a}_k \geq 0$ for any $k \leq m$, while the dominance of higher levels is equivalent to $\sum_{j=1}^k a_{ij} \geq \sum_{j=1}^k a_{i+1,j}$. But there are also non semi-algebraic relations, such as the one on the modulus of the entries. We leave the study of the variety $\mathcal{M}_{d,2}^{\text{LS}}$ for future work. Observe that the orbit argument in [AFS19, Example 2.3] does not apply since the number of segments m is greater than d .

Conjecture 2.3. *The variety of signature matrices of landscapes coincides with the variety of signature matrices of loops, that is $\mathbb{P}(\bigwedge^2 \mathbb{R}^d)$.*

Signature tensors of integrated landscapes. Since integrated landscapes are defined by integrals of non-negative functions, it is straightforward that the image of the integrated landscape embedding Φ_{ILS} consists of tensors with non-negative coefficients.

Proposition 2.4. *For any barcode B , the k -th signature tensor of F^{λ^B} is non-negative:*

$$\sigma_{i_1 \dots i_k}^{(k)}(F^{\lambda^B}) \geq 0 \quad , \quad \forall k \geq 0, \forall (i_1, \dots, i_k) \in [d]^k.$$

Note that the signature matrices of (non-integrated) landscapes can have negative coefficients: $\sigma_{ij}^{(2)}(\lambda) = \int_0^L \lambda_i(s) \dot{\lambda}_j(s) ds$ can be negative. On the other hand, integrated landscapes $F^\lambda : [0, L] \rightarrow \mathbb{R}^d$ are not loops, and their first signature is $\sigma^{(1)}(F^\lambda) = F^\lambda(L) \neq 0$. Moreover, accordingly to the characterisation of the universal variety of signature matrix $\mathcal{U}_{d,2}$ (1.7), their signature matrices are of the form $\sigma^{(2)}(F^\lambda) = \frac{1}{2}F^\lambda(L)^{\otimes 2} + Q$ for certain skew-symmetric matrices $Q \in \bigwedge^2 \mathbb{R}^d$: in particular, the symmetric part is non-zero, so the variety $\mathcal{M}_{d,2}^{\text{LS}}$ does not lie in $\mathbb{P}(\bigwedge^2 \mathbb{R}^d)$.

Despite the fact that the geometry of signature matrices of integrated landscapes seems richer, adding an integration step makes their computation heavier: indeed, for integrated landscapes one loses the piecewise-linearity which simplifies computations in the case of (non-integrated) landscapes.

3 Discrete feature maps

A discrete version of signature tensors, replacing paths with time-series, was introduced in [DET20b], and first glimpses of the related geometry appear in [BP23]. Before applying such discrete approach to persistent homology, in the following we recall definitions and we prove that discrete signatures recover time-series *uniquely up to* time-warping and time-translation.

3.1 Discrete signatures of time-series

We start by recalling the definition of discrete signature tensors as introduced in [DET20a; DET20b]. Then we propose a matrix description of the equivalence relation for time-warping and time-translation. Finally, we restate the problem of determining when two time-series have the same discrete signature in terms of the monoidal kernel, and we prove that discrete signatures recover the time-series uniquely only up to time-warping and time-translation.

Given the polynomial ring $\mathbb{R}[\mathbf{Z}] = \mathbb{R}[Z_1, \dots, Z_d]$, consider its quotient by the constant polynomials

$$\mathcal{V}_d = \mathbb{R}[Z_1, \dots, Z_d] / \mathbb{R}.$$

As (infinite dimensional) vector subspace, \mathcal{V}_d is generated by all possible monomials in the d variables. We consider the tensor algebra $\mathbb{T}(\mathcal{V}_d)$ and the power series tensor algebra $\mathbb{T}((\mathcal{V}_d))$: note that $\mathbb{T}((\mathcal{V}_d))$ can be identified to the dual space $\mathbb{T}(\mathcal{V}_d)^\vee$.

Let $\underline{\mathbf{x}} = (\mathbf{x}_1, \dots, \mathbf{x}_n)$ be a time-series of $n \geq 1$ vectors (we say, length n) in \mathbb{R}^d . We denote the set of all time-series (of any positive length) in \mathbb{R}^d by $\mathbf{TS}(\mathbb{R}^d)$. The *discrete signature map* is the map

$$\begin{aligned} \Sigma : \mathbf{TS}(\mathbb{R}^d) &\longrightarrow \mathbb{T}((\mathcal{V}_d)) \\ \underline{\mathbf{x}} &\longmapsto \Sigma(\underline{\mathbf{x}}) \end{aligned} \tag{3.1}$$

such that, for any time-series $\underline{\mathbf{x}} = (\mathbf{x}_1, \dots, \mathbf{x}_n)$ of length n , the *discrete signature* $\Sigma(\underline{\mathbf{x}})$ is the element of the tensor algebra $\mathbb{T}((\mathcal{V}_d))$ defined as follows: for any $\ell \geq 0$ and any family of monomials $p_1, \dots, p_\ell \in \mathcal{V}_d$, the coefficient of $p_1 \otimes \dots \otimes p_\ell$ in $\Sigma(\underline{\mathbf{x}})$ is

$$\langle \Sigma(\underline{\mathbf{x}}), p_1 \otimes \dots \otimes p_\ell \rangle = \begin{cases} \sum_{1 \leq i_1 < \dots < i_\ell \leq n} p_1(\mathbf{x}_{i_1+1} - \mathbf{x}_{i_1}) \dots p_\ell(\mathbf{x}_{i_\ell+1} - \mathbf{x}_{i_\ell}) & \ell \leq n-1 \\ 0 & \ell \geq n \end{cases} \quad (3.2)$$

and $\langle \Sigma(\underline{\mathbf{x}}), \epsilon \rangle = 1$ where ϵ corresponds to the empty word. The above expression is a generalisation of the notion of quasi-symmetric polynomials [DET20b, Remark 3.5]. For simplicity, we fix the notation

$$C_{p_1 \otimes \dots \otimes p_\ell}^{\underline{\mathbf{x}}} := \langle \Sigma(\underline{\mathbf{x}}), p_1 \otimes \dots \otimes p_\ell \rangle \in \mathbb{R} .$$

The *weight* of an element $p_1 \otimes \dots \otimes p_\ell$ is the sum of the degrees of the monomials p_1, \dots, p_ℓ , that is

$$\text{weight}(p_1 \otimes \dots \otimes p_\ell) := \deg(p_1) + \dots + \deg(p_\ell) . \quad (3.3)$$

The truncation *up to weight h* of the discrete signature $\Sigma(\underline{\mathbf{x}})$ is

$$\Sigma^{\leq h}(\underline{\mathbf{x}}) := \sum_{\text{weight}(p_1 \otimes \dots \otimes p_\ell) \leq h} C_{p_1 \otimes \dots \otimes p_\ell}^{\underline{\mathbf{x}}} p_1 \otimes \dots \otimes p_\ell .$$

An important feature of the (standard) signature map is being invariant under time alteration (i.e. reparametrisation of the curve). By definition, the discrete signature carries a similar property, known as *time-warping invariance* [DET20b]: it is invariant under *consecutive* time-point repetitions, that is

$$\Sigma((\mathbf{x}_1, \dots, \mathbf{x}_{j-1}, \mathbf{x}_j, \mathbf{x}_j, \mathbf{x}_{j+1}, \dots, \mathbf{x}_n)) = \Sigma((\mathbf{x}_1, \dots, \mathbf{x}_{j-1}, \mathbf{x}_j, \mathbf{x}_{j+1}, \dots, \mathbf{x}_n)) .$$

We say that a time-series is *time-warping reduced* (TWR) if it does not present consecutive repetitions. It is clear from the definition that any time-series has a unique associated TWR series so that their signatures coincide.

As the signature path (1.1) is injective modulo tree-like equivalence of paths, it is quite natural to ask under which equivalence relation the discrete signature (3.1) is injective as well. From the above, we know that time-warping is an invariant property. Moreover, again by definition (3.2), the discrete signature is also invariant under *time-translation*:

$$\Sigma((\mathbf{x}_1, \dots, \mathbf{x}_n)) = \Sigma((\mathbf{x}_1 - \mathbf{y}, \mathbf{x}_2 - \mathbf{y}, \dots, \mathbf{x}_n - \mathbf{y})) \quad , \quad \forall \mathbf{y} \in \mathbb{R}^d .$$

Let $\sim_{\text{tw}} t$ be the equivalence relation on $\mathbf{TS}(\mathbb{R}^d)$ defined by time-warping and time-translation. Let $\{\mathbf{0}\}$ be the time-series of length 1 given by the zero vector in \mathbb{R}^d . Then

$$\underline{\mathbf{y}} \sim_{\text{tw}} t \{\mathbf{0}\} \iff \underline{\mathbf{y}} = \{\mathbf{y}_1, \dots, \mathbf{y}_1\} .$$

Clearly, all the above time-series have trivial discrete signature

$$\Sigma(\{\mathbf{0}\}) = \epsilon . \quad (3.4)$$

Remark 3.1 (Matrix description of \sim_{twt}). To a time-series $\underline{\mathbf{x}} = \{\mathbf{x}_1, \dots, \mathbf{x}_n\} \in \mathbf{TS}(\mathbb{R}^d)$ we associate the matrix $\mathbf{X} = (x_{ij}) = [\mathbf{x}_1 | \dots | \mathbf{x}_n] \in \mathbb{R}^{d \times n}$. The time-translation $\underline{\mathbf{x}} \mapsto \{\mathbf{0}, \mathbf{x}_2 - \mathbf{x}_1, \dots, \mathbf{x}_n - \mathbf{x}_1\}$ corresponds to the right-multiplication below:

$$\mathbf{X} \cdot \begin{bmatrix} 0 & -1 & \cdots & -1 \\ & 1 & & \\ & & \ddots & \\ & & & 1 \end{bmatrix}_{n \times n} = \begin{bmatrix} \mathbf{0} & | & \mathbf{x}_2 - \mathbf{x}_1 & | & \dots & | & \mathbf{x}_n - \mathbf{x}_1 \end{bmatrix}. \quad (3.5)$$

On the other hand, time-warping extensions and contractions are described as follows:

$$\begin{bmatrix} \mathbf{x}_1 & | & \dots & | & \mathbf{x}_n \end{bmatrix} \cdot \begin{bmatrix} 1 & & & & \\ & 1 & 1 & & \\ & & 1 & & \\ & & & \ddots & \\ & & & & 1 \end{bmatrix}_{n \times (n+1)} = \begin{bmatrix} \mathbf{x}_1 & | & \mathbf{x}_2 & | & \mathbf{x}_2 & | & \mathbf{x}_3 & | & \dots & | & \mathbf{x}_n \end{bmatrix} \quad (3.6)$$

$$\begin{bmatrix} \mathbf{x}_1 & | & \mathbf{x}_2 & | & \mathbf{x}_2 & | & \mathbf{x}_3 & | & \dots & | & \mathbf{x}_n \end{bmatrix} \cdot \begin{bmatrix} 1 & & & & \\ & 1 & -1 & & \\ & & 1 & & \\ & & & 1 & \\ & & & & \ddots & \\ & & & & & 1 \end{bmatrix}_{(n+1) \times n} = \begin{bmatrix} \mathbf{x}_1 & | & \mathbf{x}_2 & | & \mathbf{x}_3 & | & \dots & | & \mathbf{x}_n \end{bmatrix}. \quad (3.7)$$

Finally, the time-series of consecutive differences $\Delta \underline{\mathbf{x}}$ is obtained by:

$$\mathbf{X} \cdot \begin{bmatrix} -1 & & & \\ 1 & -1 & & \\ & 1 & \ddots & \\ & & \ddots & -1 \\ & & & 1 \end{bmatrix}_{n \times (n-1)} = \begin{bmatrix} \mathbf{x}_2 - \mathbf{x}_1 & | & \dots & | & \mathbf{x}_n - \mathbf{x}_{n-1} \end{bmatrix}. \quad (3.8)$$

Similarly to concatenation of paths, one can consider a *shifted* concatenation of time-series: for any two time-series $\underline{\mathbf{x}} = \{\mathbf{x}_1, \dots, \mathbf{x}_n\}$ and $\underline{\mathbf{y}} = \{\mathbf{y}_1, \dots, \mathbf{y}_m\}$ in \mathbb{R}^d , their (shifted) *concatenation* is the time-series of length $n + m$

$$\begin{aligned} \{\underline{\mathbf{x}} | \underline{\mathbf{y}}\} &:= \begin{cases} \mathbf{x}_k & k \in [n] \\ \mathbf{y}_{k-n} - \mathbf{y}_1 + \mathbf{x}_n & k \in [n+m] \setminus [n] \end{cases} \\ &= \{\mathbf{x}_1, \dots, \mathbf{x}_n, \mathbf{x}_n, \mathbf{y}_2 - \mathbf{y}_1 + \mathbf{x}_n, \dots, \mathbf{y}_m - \mathbf{y}_1 + \mathbf{x}_n\} \end{aligned} \quad (3.9)$$

The shift in the formula (3.9) is motivated by the need of emulating the Chen relation (1.3). Indeed, for discrete signatures of time-series the following *discrete Chen relation* holds (cf. [BP23, Theorem 3.6]):

$$\Sigma(\{\underline{\mathbf{x}} | \underline{\mathbf{y}}\}) = \Sigma(\underline{\mathbf{x}}) \otimes \Sigma(\underline{\mathbf{y}}). \quad (3.10)$$

Note that the shifted concatenation of time-series is coherent with the time-warping-translation equivalence. Moreover, the class $\{\mathbf{0}\}$ (modulo \sim_{twt}) is the identity element in $\mathbf{TS}(\mathbb{R}^d)$ for the shifted concatenation:

$$\{\{\mathbf{0}\} | \underline{\mathbf{x}}\} = \{\underline{\mathbf{x}} | \{\mathbf{0}\}\} = \underline{\mathbf{x}}.$$

Finally, $\mathbf{TS}(\mathbb{R}^d)$ is a *monoid* with respect to the shift concatenation with identity element $\{\mathbf{0}\}$, and the discrete signature map (3.1) is a *monoid homomorphism* (in light of (3.10) and (3.4)). Now, determining when two time-series have the same discrete signature is equivalent to determine the kernel of the monoid homomorphism Σ

$$\ker(\Sigma) := \{(\underline{\mathbf{x}}, \underline{\mathbf{y}}) \in \mathbf{TS}(\mathbb{R}^d)^2 \mid \Sigma(\underline{\mathbf{x}}) = \Sigma(\underline{\mathbf{y}})\} .$$

Note that this is different from determining which time-series have trivial discrete signature ϵ . We claim that $\ker(\Sigma)$ corresponds to the diagonal in $(\mathbf{TS}(\mathbb{R}^d)/\sim_{\text{tw}})^2$, and hence the (quotient) discrete signature map $\mathbf{TS}(\mathbb{R}^d)/\sim_{\text{tw}} \rightarrow \mathbb{T}(\mathcal{V}_d)$ is injective.

In the case of the classical Chen signatures, the bijection between tree-like equivalence for paths and the Chen signatures is obtained by exploiting the group structure of paths and the Chen relation (1.3) making the signature path map (1.1) a group homomorphism. For discrete signature we just have a monoid structure, so determining the (monoidal) kernel $\ker(\Sigma)$ requires a different approach. First, we observe that TWR time-series with same discrete signatures must have the same length.

Given a time-series $\underline{\mathbf{x}} = \{\mathbf{x}_1, \dots, \mathbf{x}_n\} \in \mathbf{TS}(\mathbb{R}^d)$ we call *difference time-series* the time-series of consecutive differences

$$\Delta \underline{\mathbf{x}} := (\Delta \mathbf{x}_1, \dots, \Delta \mathbf{x}_{n-1}) \quad \text{where } \Delta \mathbf{x}_j := \mathbf{x}_{j+1} - \mathbf{x}_j .$$

Lemma 3.2. *Let $\underline{\mathbf{x}}, \underline{\mathbf{y}} \in \mathbf{TS}(\mathbb{R}^d)$ be two TWR time-series of lengths n and m , respectively. If $\Sigma(\underline{\mathbf{x}}) = \Sigma(\underline{\mathbf{y}})$, then $n = m$.*

Proof. Assume, by contradiction, that $m < n$ (similar argument applies to $n < m$). We extend $\underline{\mathbf{y}}$ to its time-warped equivalent time-series $\underline{\mathbf{y}} = \{\mathbf{y}_1, \dots, \mathbf{y}_m, \mathbf{y}_m, \dots, \mathbf{y}_m\}$ of length n . We identify $\underline{\mathbf{x}}$ and $\underline{\mathbf{y}}$ with the $d \times (n-1)$ matrices $(\Delta x_{ij}) = (x_{ij+1} - x_{ij})$ and $(\Delta y_{ij}) = (y_{ij+1} - y_{ij})$: note that the last $m - n - 1$ columns of (Δy_{ij}) are zero. Since $\underline{\mathbf{x}}$ is TWR, (Δx_{ij}) doesn't have a zero column, so there exists a sequence $(i_1, \dots, i_n) \subset [d]^n$ such that $\Delta x_{i_1 1}, \Delta x_{i_2 2}, \dots, \Delta x_{i_n n}$ are nonzero entries. In particular, it holds

$$C_{Z_{i_1} \otimes Z_{i_2} \otimes \dots \otimes Z_{i_n}}^{\underline{\mathbf{x}}} = \Delta x_{i_1 1} \cdot \Delta x_{i_2 2} \cdots \Delta x_{i_n n} \neq 0 .$$

On the other hand, by construction $\Delta y_{i_n n} = 0$, so $C_{Z_{i_1} \otimes Z_{i_2} \otimes \dots \otimes Z_{i_n}}^{\underline{\mathbf{y}}} = 0$. This contradicts the hypothesis $\Sigma(\underline{\mathbf{x}}) = \Sigma(\underline{\mathbf{y}})$. \square

Lemma 3.3. *For any two one-dimensional time-series $\underline{\mathbf{x}}, \underline{\mathbf{y}} \in \mathbf{TS}(\mathbb{R})$ it holds*

$$\Sigma(\underline{\mathbf{x}}) = \Sigma(\underline{\mathbf{y}}) \iff \underline{\mathbf{x}} \sim_{\text{tw}} \underline{\mathbf{y}} .$$

In particular, the quotient map $\mathbf{TS}(\mathbb{R})/\sim_{\text{tw}} \hookrightarrow \mathbb{T}(\mathcal{V}_1)$ is injective.

Proof. Let $\underline{\mathbf{x}} = (x_1, \dots, x_n)$ and $\underline{\mathbf{y}} = (y_1, \dots, y_m)$ be 1-dimensional time-series in $\mathbf{TS}(\mathbb{R})$ such that $\Sigma(\underline{\mathbf{x}}) = \Sigma(\underline{\mathbf{y}})$. Since the discrete signature is time-warping invariant, we may assume them to be TWR. From Lemma 3.2, we know that $n = m$. By TWR assumption, there are no zeros in the corresponding time-series of consecutive

differences $\Delta \mathbf{x} = (\Delta x_j) = (x_{j+1} - x_j)$ and $\Delta \mathbf{y} = (\Delta y_j) = (y_{j+1} - y_j)$. We assume that $\Sigma(\mathbf{x}) = \Sigma(\mathbf{y})$, and show that it has to hold $\mathbf{x} = \mathbf{y}$. Let $Z^{\otimes h} := Z \otimes \dots \otimes Z$ the tensor product of h copies of the monomial $Z \in \mathbb{R}[Z]$.

Claim 1: $\Delta \mathbf{x}$ and $\Delta \mathbf{y}$ coincide up to permutation of their time-points. Since $\Sigma(\mathbf{x}) = \Sigma(\mathbf{y})$, for any $h \in [n-1]$ it holds

$$C_{Z^{\otimes h}}^{\mathbf{x}} = C_{Z^{\otimes h}}^{\mathbf{y}} .$$

These are all the elementary symmetric functions in $\Delta \mathbf{x}$ and $\Delta \mathbf{y}$ respectively. It follows that they define the same univariate monic polynomial

$$f_{\Delta \mathbf{x}} := T^n + \sum_{h=1}^{n-1} (-1)^h C_{Z^{\otimes h}}^{\mathbf{x}} T^{n-h} = T^n + \sum_{k=1}^{n-1} (-1)^k C_{Z^{\otimes k}}^{\mathbf{y}} T^{n-k} =: f_{\Delta \mathbf{y}} .$$

In particular, the set of roots $\Delta \mathbf{x}$ and $\Delta \mathbf{y}$ coincide (as unordered sets), hence $\Delta \mathbf{x}$ and $\Delta \mathbf{y}$ coincide up to permutation as ordered sets.

Claim 2: $\mathbf{x} = \mathbf{y}$ as time-series. For simplicity, and in light of Claim 1, we write $\Delta \mathbf{x} = (p_1, \dots, p_{n-1})$ and $\Delta \mathbf{y} = (p_{\sigma(1)}, \dots, p_{\sigma(n-1)})$ for a certain permutation $\sigma \in \mathfrak{S}_{n-1}$. For any $j \in [n-1]$ we consider the element $\mathcal{Z}_j := Z^{\otimes(j-1)} \otimes Z^2 \otimes Z^{\otimes(n-1-j)} \in \mathbb{T}((\mathcal{V}))$ (with $n-1$ tensor entries). The hypothesis $\Sigma(\mathbf{x}) = \Sigma(\mathbf{y})$ implies

$$p_1 \cdots p_{j-1} p_j^2 p_{j+1} \cdots p_{n-1} = C_{\mathcal{Z}}^{\mathbf{x}} = C_{\mathcal{Z}}^{\mathbf{y}} = p_{\sigma(1)} \cdots p_{\sigma(j)}^2 \cdots p_{\sigma(n-1)} .$$

Since \mathbf{x} and \mathbf{y} are TWR, each p_i is non-zero, and the above equality implies $p_j^2 p_{\sigma(j)} = p_j p_{\sigma(j)}^2$, hence $p_j = p_{\sigma(j)}$. This holds for any $j \in [n-1]$, that is $\Delta \mathbf{x} = \Delta \mathbf{y}$ as ordered sets. We conclude $\mathbf{x} = \mathbf{y} + \{a, \dots, a\}$ for a certain $a \in \mathbb{R}$. \square

Theorem 3.4. *For any two time-series $\underline{\mathbf{x}}, \underline{\mathbf{y}} \in \mathbf{TS}(\mathbb{R}^d)$ it holds*

$$\Sigma(\underline{\mathbf{x}}) = \Sigma(\underline{\mathbf{y}}) \iff \underline{\mathbf{x}} \sim_{\text{twt}} \underline{\mathbf{y}} .$$

In particular, the quotient map $\mathbf{TS}(\mathbb{R}^d)/\sim_{\text{twt}} \hookrightarrow \mathbb{T}((\mathcal{V}_d))$ is injective.

Remark 3.5. The above theorem was already proved in [DET22, Theorem 3.15] in a more general setting. However, we proved it independently and became aware of the aforementioned reference only after a discussion with Diehl, Ebrahimi-Fard and Tapia, whom we thank.

Proof. Let $\underline{\mathbf{x}}, \underline{\mathbf{y}} \in \mathbf{TS}(\mathbb{R}^d)$ be such that $\Sigma(\underline{\mathbf{x}}) = \Sigma(\underline{\mathbf{y}})$. By invariance of the discrete signature under time-warping, we may assume them to be TWR. From Lemma 3.2 we know that $\underline{\mathbf{x}}$ and $\underline{\mathbf{y}}$ must have same length n . Let $\underline{\mathbf{x}} = \{\mathbf{x}_1, \dots, \mathbf{x}_n\}$ and $\underline{\mathbf{y}} = \{\mathbf{y}_1, \dots, \mathbf{y}_n\}$.

For every $i \in [d]$ consider the one-dimensional time-series $\underline{\mathbf{x}}^i := \{x_{i1}, \dots, x_{in}\}$ and $\underline{\mathbf{y}}^i := \{y_{i1}, \dots, y_{in}\}$ of the i -th vector entries. Observe that they may not be TWR, even if the d -dimensional time-series are so. Since $\langle \Sigma(\underline{\mathbf{x}}), p_1(Z_i) \otimes \dots \otimes p_\ell(Z_i) \rangle =$

$\langle \Sigma(\underline{\mathbf{x}}^i), p_1(Z_i) \otimes \dots \otimes p_\ell(Z_i) \rangle$ (and similar for $\underline{\mathbf{y}}$), it holds $\Sigma(\underline{\mathbf{x}}^i) = \Sigma(\underline{\mathbf{y}}^i)$ (these are discrete signatures of one-dimensional time-series). Then from Lemma 3.3 we get $\underline{\mathbf{x}}^i \sim_{\text{twt}} \underline{\mathbf{y}}^i$. However, this is not enough for concluding that $\underline{\mathbf{x}}$ and $\underline{\mathbf{y}}$ are equivalent. We still need to prove two facts. First, as $i \in [d]$ varies, $\underline{\mathbf{x}}^i$ and $\underline{\mathbf{y}}^i$ must admit time-warping contractions along the same entries. Second, $\underline{\mathbf{x}}^i$ and $\underline{\mathbf{y}}^i$ must be time-translated with respect to the same scalar for all $i \in [d]$.

For any $i \in [d]$ consider the difference time-series $\Delta \underline{\mathbf{x}}^i$ and $\Delta \underline{\mathbf{y}}^i$. Since $\underline{\mathbf{x}}^i$ and $\underline{\mathbf{y}}^i$ are not necessarily TWR, their difference time-series may contain zeros. However, *Claim 1* in the proof of Lemma 3.3 still applies, so that $\Delta \underline{\mathbf{x}}^i$ is a permutation of $\Delta \underline{\mathbf{y}}^i$. In particular, they contain the same number of zeros. Moreover, applying *Claim 2* (from the same proof) to their time-warping reductions implies that non-zero values in $\Delta \underline{\mathbf{x}}^i$ and $\Delta \underline{\mathbf{y}}^i$ appear in the same order in both difference time-series. It follows that $\underline{\mathbf{x}}^i$ and $\underline{\mathbf{y}}^i$ may differ only in the order of appearance of the zeros.

For the same argument in Lemma 3.2, since the d -dimensional time-series $\underline{\mathbf{x}}$ is TWR, the difference time-series $\Delta \underline{\mathbf{x}}$ doesn't have zero-columns, hence there exists $(i_1, \dots, i_n) \subset [d]^n$ such that $C_{Z_{i_1} \otimes \dots \otimes Z_{i_n}}^{\underline{\mathbf{x}}} = \Delta x_{i_1 1} \cdots \Delta x_{i_n n} \neq 0$ (in particular, each $\Delta x_{i_j j} \neq 0$). Since the time-series have the same discrete signatures, it follows $C_{Z_{i_1} \otimes \dots \otimes Z_{i_n}}^{\underline{\mathbf{y}}} = \Delta y_{i_1 1} \cdots \Delta y_{i_n n}$ is non-zero too, as well as each $\Delta y_{i_j j}$. Now, pick $(\bar{i}, \bar{j}) \in [d] \times n$ such that $\Delta x_{\bar{i} \bar{j}} = 0$ and substitute in the above tensor-monomials $Z_{i_j \bar{j}}$ with $Z_{\bar{i} \bar{j}}$: one gets

$$\begin{aligned} 0 &= \Delta x_{i_1 1} \cdots \Delta x_{i_{\bar{j}-1} \bar{j}-1} \cdot \Delta x_{\bar{i} \bar{j}} \cdot \Delta x_{i_{\bar{j}+1} \bar{j}} \cdots \Delta x_{i_n n} \\ &= \underbrace{\Delta y_{i_1 1} \cdots \Delta y_{i_{\bar{j}-1} \bar{j}-1}}_{\neq 0} \cdot \Delta y_{\bar{i} \bar{j}} \cdot \underbrace{\Delta y_{i_{\bar{j}+1} \bar{j}} \cdots \Delta y_{i_n n}}_{\neq 0} \end{aligned}$$

implying $\Delta y_{\bar{i} \bar{j}} = 0$. This shows that the one-dimensional difference time-series $\Delta \underline{\mathbf{x}}^i$ and $\Delta \underline{\mathbf{y}}^i$ have zeros in the same entries, hence they coincide. We conclude that $\Delta \underline{\mathbf{x}} = \Delta \underline{\mathbf{y}}$, that is $\underline{\mathbf{x}} \sim_{\text{twt}} \underline{\mathbf{y}}$. \square

Remark 3.6 (Refinement of segment decomposition). For data applications, unlike the classical signature of paths, the discrete signature is not invariant under “refinement of segment decomposition”, which would correspond to an expansion of the time-series: an evidence is given by the discrete Chen relation (3.10). However, the two signatures are interrelated [DET20b, Proposition 5.5]: given a bounded variation path $\gamma : [0, 1] \rightarrow \mathbb{R}^d$, the limit —over finite partitions $\pi = \{0 < t_1 < \dots < t_n < 1\}$ — of the discrete signatures of the time-series $\underline{\mathbf{x}}^\pi := \{\gamma(0), \gamma(t_1), \dots, \gamma(t_n), \gamma(1)\}$ converges to the Chen signature of γ .

3.2 The discrete landscape feature map

The discrete signature is a well-defined and meaningful descriptor for persistence landscapes (and in general, of PWL paths). Indeed, persistence landscapes come with a “canonical” time-series associated to them, namely the *minimal segment decomposition* (cf. Definition 1.3).

Each level $\lambda_k(t)$ of a persistence landscape λ is a piecewise linear function with

slope 1, -1 , or 0. The *critical points* of λ_k are the values of t at which the slope changes, and the *critical points* of the landscape λ is the union of all the critical points for each λ_k . A persistence landscape is completely determined by its critical points. In fact, the standard implementation of landscape methods keeps track of the critical points rather than the landscape as a function [BD17]. One can list the critical points of a landscape in terms of the corresponding barcode as follows.

Lemma 3.7 ([Bub20], Lemma 5.8). *Given a barcode $B = \{(b_i, d_i)\}$, the critical points in the corresponding landscape λ^B consist of*

1. *the left endpoints b_i ,*
2. *the right endpoints d_i ,*
3. *the midpoints $\frac{b_i + d_i}{2}$,*
4. *the midpoints $\frac{b_i + b_j}{2}$ of pairs of bars where $b_k < b_i < d_j < d_i$.*

Evaluating a landscape at all of its critical points, i.e. computing the critical values of $\lambda = (\lambda_1, \dots, \lambda_d)$, produces a times-series $\underline{\lambda} \in \mathbf{TS}(\mathbb{R}^d)$ whose length is given by the number of critical points.

Remark 3.8. In practice, we will work with landscapes with a fixed number of levels, say d , where we truncate levels, or extend levels that are identically zero as necessary to reach d levels.

The assumption in the above remark allows us to associate a time-series to a landscape (hence to a barcode) in a canonical way. We call this *discrete landscape embedding* and denote it by

$$I : \mathbf{Bar} \rightarrow \mathbf{TS}(\mathbb{R}^d) \quad (3.11)$$

Analogous to the feature maps in Subsection 1.2, we define the *discrete landscape feature map* as the composition of the discrete signature and the discrete landscape embedding:

$$\Phi_I : \mathbf{Bar} \xrightarrow{I} \mathbf{TS}(\mathbb{R}^d) \xrightarrow{\Sigma} \mathbb{T}((\mathcal{V}_d)). \quad (3.12)$$

The following naive example illustrates how the discrete feature map distinguish between landscapes that are tree-like equivalent.

Example 3.9. Consider the singleton barcode $B = \{(b, d)\}$. Then $I(B) = (0, \frac{d-b}{2}, 0)$ is a one-dimensional time-series of length 3 whose discrete signature up to weight 3

is

$$\begin{aligned}
\langle \Phi_I(B), Z \rangle &= 0 \\
\langle \Phi_I(B), Z^2 \rangle &= \frac{(d-b)^2}{2} \\
\langle \Phi_I(B), Z \otimes Z \rangle &= -\frac{(d-b)^2}{2^2} \\
\langle \Phi_I(B), Z^3 \rangle &= 0 \\
\langle \Phi_I(B), Z^2 \otimes Z \rangle &= -\frac{(d-b)^3}{2^3} \\
\langle \Phi_I(B), Z \otimes Z^2 \rangle &= \frac{(d-b)^3}{2^3} \\
\langle \Phi_I(B), Z \otimes Z \otimes Z \rangle &= 0 .
\end{aligned}$$

Now consider a barcode $C = \{(b, d), (b', d')\}$ where $b' > d$ (similar to Figure 1.2). Then, up to *twt*-equivalence,

$$I(C) = \left(0, \frac{d-b}{2}, 0, \frac{d'-b'}{2}, 0 \right)$$

is a one-dimensional time-series of length 5 whose signature up to weight 3 is

$$\begin{aligned}
\langle \Phi_I(C), Z \rangle &= 0 \\
\langle \Phi_I(C), Z^2 \rangle &= \frac{1}{2} ((d-b)^2 + (d'-b')^2) \\
\langle \Phi_I(C), Z \otimes Z \rangle &= -\frac{1}{2^2} ((d-b)^2 + (d'-b')^2) \\
\langle \Phi_I(C), Z^3 \rangle &= 0 \\
\langle \Phi_I(C), Z^2 \otimes Z \rangle &= -\frac{1}{2^3} ((d-b)^3 + (d'-b')^3) \\
\langle \Phi_I(C), Z \otimes Z^2 \rangle &= \frac{1}{2^3} ((d-b)^3 + (d'-b')^3) \\
\langle \Phi_I(C), Z \otimes Z \otimes Z \rangle &= 0 .
\end{aligned}$$

In slightly more generality, whenever a barcode B has a landscape λ^B with a single level, the discrete signature captures persistence, but does not capture additional information beyond it.

Lemma 3.10. *The signature of a barcode B defining a single-level landscape λ^B is completely determined by the persistence of the bars in B .*

Proof. If λ^B has a single level then there exists a total ordering \prec of B so that $d \leq b'$ whenever $(d, b) \prec (d', b')$, since otherwise there would be a second level. Label the barcodes in such a way that $(b_1, d_1) < (b_2, d_2) < \dots < (b_{|B|}, d_{|B|})$, with $d_i < b_j$ if $i < j$. Then the time-series of differences has the form

$$\Delta I(B) = \left(\frac{(d_1 - b_1)}{2}, \frac{-(d_1 - b_1)}{2}, \frac{(d_2 - b_2)}{2}, \frac{-(d_2 - b_2)}{2}, \dots, \frac{(d_{|B|} - b_{|B|})}{2}, \frac{-(d_{|B|} - b_{|B|})}{2} \right).$$

Since the signature is obtained by evaluation of polynomials on the time-series of differences, the lemma follows. \square

Corollary 3.11. *The coefficients corresponding to univariate polynomials $p \in \mathbb{R}[Z_i]$ are determined by the persistence.*

One can derive some explicit signature coefficients in terms of persistence for single-level landscapes. For example, straightforward computations with the difference time-series in the proof above give

$$\begin{aligned} \langle \Phi_I(B), Z^{\otimes n} \rangle &= 0 && \text{if } n \equiv 1 \pmod{2} \\ \langle \Phi_I(B), Z^n \rangle &= \begin{cases} 0 & \text{if } n \equiv 1 \pmod{2} \\ \sum_{\beta \in B} \frac{(d_\beta - b_\beta)^n}{2^{n-1}} & \text{if } n \equiv 0 \pmod{2} \end{cases} \end{aligned}$$

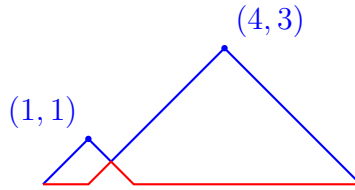
Remark 3.12. The latter equation can be interpreted as a list of even moments of the time-series, so that standard statistical descriptors of time-series are naturally captured by the discrete signature. In particular, going back to the example in Figure 1.2, the above observation shows that the discrete signature encodes information about the persistence of the spheres, which is determined by their radii, whereas the Chen signature is trivial.

The dependence of the signature on persistence alone is specific to one-level landscapes. For landscapes with more levels the signature encodes additional information related to relative distances between bars, and this is picked up already at weight 2.

Example 3.13. Consider the time-series

$$\underline{\mathbf{x}} = \left(\begin{pmatrix} 0 \\ 0 \end{pmatrix}, \begin{pmatrix} 1 \\ 0 \end{pmatrix}, \begin{pmatrix} 1/2 \\ 1/2 \end{pmatrix}, \begin{pmatrix} 1 \\ 0 \end{pmatrix}, \begin{pmatrix} 3 \\ 0 \end{pmatrix}, \begin{pmatrix} 0 \\ 0 \end{pmatrix} \right)$$

corresponding to the landscape



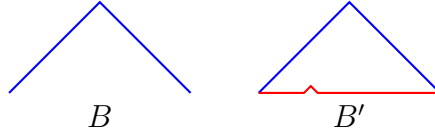
The discrete signature of $\underline{\mathbf{x}}$ up to weight 2 is

$$\begin{aligned}
\langle \Sigma(\underline{\mathbf{x}}), Z_1 \rangle &= \langle \Sigma(\underline{\mathbf{x}}), Z_2 \rangle = 0 \\
\langle \Sigma(\underline{\mathbf{x}}), Z_1^2 \rangle &= \frac{29}{2} \\
\langle \Sigma(\underline{\mathbf{x}}), Z_1 Z_2 \rangle &= -\frac{1}{2} \\
\langle \Sigma(\underline{\mathbf{x}}), Z_2^2 \rangle &= \frac{1}{2} \\
\langle \Sigma(\underline{\mathbf{x}}), Z_1 \otimes Z_1 \rangle &= -\frac{29}{4} \\
\langle \Sigma(\underline{\mathbf{x}}), Z_1 \otimes Z_2 \rangle &= \frac{1}{4} \\
\langle \Sigma(\underline{\mathbf{x}}), Z_2 \otimes Z_2 \rangle &= -\frac{1}{4} .
\end{aligned}$$

3.3 Continuity of the discrete landscape feature map

The discrete signature, being a component-wise polynomial map, is continuous. However, the discrete landscape embedding is not, hence the discrete landscape feature map is not continuous either. The key obstruction is illustrated in the following example.

Example 3.14. Let $B = \{(b, d)\}$, with $d > b$, and $B' = \{(b, d), (\frac{d-b}{4}, \frac{d-b}{4}\delta)\}$ for some $0 < \delta << d-b$. Their bottleneck distance (cf. Section 3.4) is $\text{dist}_{\mathbf{B}}(B, B') = \frac{\delta}{\sqrt{2}}$, and the corresponding persistence landscapes are



Some coefficients in the discrete signatures are such that no choice of δ will make their difference small. For instance,

$$\begin{aligned}
\langle \Phi_I(B), Z_1 \otimes Z_1 \otimes Z_1 \rangle &= 0 \\
\langle \Phi_I(B'), Z_1 \otimes Z_1 \otimes Z_1 \rangle &= -\frac{(d-b)^3}{2^5} + o(\delta) .
\end{aligned}$$

The heart of the issue with continuity is the poor behaviour of the discrete signature under refinement of segment decomposition (cf. Remark 3.6). Indeed, in the above example, the inclusion of a bar with arbitrarily small persistence, which produces a barcode that is close in bottleneck distance, forces a refinement of segment decomposition, whence the discontinuity.

3.4 The specialised discrete landscape feature map

For applications, one may want to compare barcodes using signatures as input for machine learning methods [LM25]. In light of this, it makes sense to consider a finite subset $D \subset \mathbf{Bar}$. Then we can modify the discrete embedding map $I : \mathbf{Bar} \rightarrow \mathbf{TS}(\mathbb{R}^d)$ (3.11) as follows. Consider the union of all critical points of the landscapes arising from the domain D

$$C_D := \{c_1, c_2, \dots, c_N\} = \{c \mid c \text{ critical point of } \lambda^B \text{ for some } B \in D\} ,$$

and define the *specialised discrete embedding map*

$$\begin{array}{ccccc} I_D : & D & \rightarrow & \mathbf{BV}([0, L], \mathbb{R}^d) & \rightarrow & \mathbf{TS}(\mathbb{R}^d) \\ & B & \mapsto & \lambda^B & \mapsto & (\lambda^B(c_1), \lambda^B(c_2), \dots, \lambda^B(c_N)) . \end{array} \quad (3.13)$$

This restriction allows us to have a consistent segment subdivision of the landscapes across all barcodes in D , which then guarantees continuity of the *specialised discrete landscape feature map*

$$\Phi_{I_D}^{\leq k} : D \xrightarrow{I_D} \mathbf{TS}(\mathbb{R}^d) \xrightarrow{\Sigma^{\leq k}} \mathbb{T}^{\leq k}((\mathcal{V}_d)) \quad (3.14)$$

where $\mathbb{T}^{\leq k}((\mathcal{V}_d))$ denotes the space of discrete signature tensors truncated at weight k .

For practical purposes, a particularly desirable property of a feature map would be stability, or equivalently being 1-Lipschitz. A weaker but still desirable condition is uniform continuity. We aim that the specialised discrete landscape feature map $\Phi_{I_D}^{\leq k}$ is uniformly continuous. Before proving this, we describe explicitly the metrics on all the involved spaces, that is \mathbf{Bar} , $\mathbf{BV}([0, L], \mathbb{R}^d)$, $\mathbf{TS}(\mathbb{R}^d)$ and $\mathbb{T}^{\leq k}((\mathcal{V}_d))$.

Bottleneck distance. The *bottleneck distance* was classically introduced for persistence diagrams in [CEH07, Sec. 3], and it translates in the following distance between barcodes:

$$\text{dist}_{\mathbf{B}}(B, B') := \inf_{\sigma: B \xrightarrow{1:1} B'} \sup_{B_i \in B} \|B_i - \sigma(B_i)\|_{\infty} .$$

The distance between landscapes is the ∞ -norm $\|\cdot\|_{\infty}$, as considered in [Bub15, Sec. 5]:

$$\text{dist}_{\infty}(\lambda^B, \lambda^{B'}) := \left\| \lambda^B - \lambda^{B'} \right\|_{\infty} = \sup_t \left\{ \left\| \lambda^B(t) - \lambda^{B'}(t) \right\|_2 \right\} .$$

Finally, given two time-series in \mathbb{R}^d of the same length n , the distance between them that we consider is

$$\text{dist}_{\mathbf{TS}}(\underline{\mathbf{x}}, \underline{\mathbf{y}}) = \max \{ \|\mathbf{x}_i - \mathbf{y}_i\|_2 \mid i \in [n] \} .$$

Bombieri-Weyl product. The (non-degenerate) scalar product $\langle \cdot, \cdot \rangle$ on \mathbb{R}^d defining the 2-norm $\|\cdot\|_2$ naturally induces a scalar product on $\mathbb{T}^{\leq k}(\mathcal{V}_d)$, called *Bombieri-Weyl product*. Fix an orthonormal basis (e_1, \dots, e_d) of \mathbb{R}^d . Let $Sym^\bullet \mathbb{R}^d$ be the graded symmetric algebra over \mathbb{R}^d , which is isomorphic (as graded algebras) to the polynomial ring $\mathbb{R}[Z_1, \dots, Z_d]$: one identifies the basis vector e_i with the variable Z_i . In particular, the isomorphism restricts to each graded component, so that $Sym^h \mathbb{R}^d$ is isomorphic to the vector space $\mathbb{R}[Z_1, \dots, Z_d]_h$ of homogeneous polynomials in d variables of degree h . For any $h \geq 0$, the scalar product $\langle \cdot, \cdot \rangle$ extends to a scalar product, called *Bombieri-Weyl product* (BW-product), on $\mathbb{R}[Z_1, \dots, Z_d]_h$ defined on the monomials (and extended by linearity) by

$$\langle Z_1^{\alpha_1} \dots Z_d^{\alpha_d}, Z_1^{\beta_1} \dots Z_d^{\beta_d} \rangle_{sym} = \binom{h}{\alpha}^{-1} \delta_{\alpha\beta},$$

where $\binom{h}{\alpha} = \frac{h!}{\alpha_1! \dots \alpha_d!}$ and the latter symbol is the Kronecker symbol. The BW-product on $Sym^h \mathbb{R}^d$ induces the Bombieri-Weyl norm, also known as *Kostlan norm*: for any degree- h monomial $\mathbf{Z}^\alpha := Z_1^{\alpha_1} \dots Z_d^{\alpha_d}$ it holds

$$\|\mathbf{Z}^\alpha\|_{sym}^2 = \binom{h}{\alpha}^{-1}.$$

One extends the BW-product to the whole algebra $Sym^\bullet \mathbb{R}^d \simeq \mathbb{R}[Z_1, \dots, Z_d]$ by imposing orthogonality between monomials with different grades. This defines a scalar product on \mathcal{V}_d . Again, this extends to any tensor-power of $\mathcal{V}_d^{\otimes \ell}$, resulting in the following norm: given ℓ monomials $\mathbf{Z}^{\alpha_1}, \dots, \mathbf{Z}^{\alpha_\ell}$ in \mathcal{V}_d such that each $\alpha_i = (\alpha_{i,1}, \dots, \alpha_{i,d}) \in \mathbb{N}^d$ is a partition of the degree $|\alpha_i| = \alpha_{i,1} + \dots + \alpha_{i,d}$, it holds

$$\|\mathbf{Z}^{\alpha_1} \otimes \dots \otimes \mathbf{Z}^{\alpha_\ell}\|_{BW}^2 = \|\mathbf{Z}^{\alpha_1}\|_{sym}^2 \dots \|\mathbf{Z}^{\alpha_\ell}\|_{sym}^2 = \binom{|\alpha_1|}{\alpha_1}^{-1} \dots \binom{|\alpha_\ell|}{\alpha_\ell}^{-1}.$$

Analogously, one extends the scalar product to $\mathbb{T}^{\leq k}(\mathcal{V}_d)$ by imposing orthogonality between tensor-products of different order. In particular, the BW-norm on $\mathbb{T}^{\leq k}(\mathcal{V}_d)$ is

$$\left\| \sum_{|\alpha_1| + \dots + |\alpha_\ell| \leq k} C_{\alpha_1, \dots, \alpha_\ell} \mathbf{Z}^{\alpha_1} \otimes \dots \otimes \mathbf{Z}^{\alpha_\ell} \right\|_{BW}^2 = \sum_{|\alpha_1| + \dots + |\alpha_\ell| \leq k} C_{\alpha_1, \dots, \alpha_\ell}^2 \binom{|\alpha_1|}{\alpha_1}^{-1} \dots \binom{|\alpha_\ell|}{\alpha_\ell}^{-1}.$$

This allows to define the following *Bombieri-Weyl distance* on $\mathbb{T}^{\leq k}(\mathcal{V}_d)$: given two elements $f, g \in \mathbb{T}^{\leq k}(\mathcal{V}_d)$ with coefficients $C_{\alpha_1, \dots, \alpha_\ell}^f$ and $C_{\alpha_1, \dots, \alpha_\ell}^g$ respectively, it holds

$$\begin{aligned} \text{dist}_{BW}(f, g) &= \left\| \sum_{|\alpha_1| + \dots + |\alpha_\ell| \leq k} (C_{\alpha_1, \dots, \alpha_\ell}^f - C_{\alpha_1, \dots, \alpha_\ell}^g) \mathbf{Z}^{\alpha_1} \otimes \dots \otimes \mathbf{Z}^{\alpha_\ell} \right\|_{BW}^2 \\ &= \sum_{|\alpha_1| + \dots + |\alpha_\ell| \leq k} (C_{\alpha_1, \dots, \alpha_\ell}^f - C_{\alpha_1, \dots, \alpha_\ell}^g)^2 \binom{|\alpha_1|}{\alpha_1}^{-1} \dots \binom{|\alpha_\ell|}{\alpha_\ell}^{-1} \end{aligned} \quad (3.15)$$

Uniform continuity. In our case we start from the standard scalar product $\langle \mathbf{u}, \mathbf{w} \rangle = \sum u_i w_i$ on \mathbb{R}^d , defining the 2-norm $\|\cdot\|_2$.

Theorem 3.15. *Given $D \subset \mathbf{Bar}$ a finite set of barcodes, the specialised discrete landscape feature map $\Phi_{I_D}^{\leq k}$ (3.14) is uniformly continuous with respect to the bottleneck distance on \mathbf{Bar} and the Bombieri-Weyl distance on $\mathbb{T}^{\leq k}((\mathcal{V}_d))$.*

Proof. We divide the proof in more steps, showing that each map involved in $\Phi_{I_D}^{\leq k}$ is uniformly continuous.

Claim 1: The discrete embedding I_D is uniformly continuous. The map I_D can be factored as $I_d = \mathbf{ev} \circ \lambda$ where $\lambda : D \rightarrow \mathbf{BV}(\mathbb{R}^d)$ is the persistence landscape map restricted to D , and \mathbf{ev} is evaluation at all the points in C_D .

In [Bub20, Theorem 2.4], it was shown that λ is stable, meaning 1-Lipschitz where $\mathbf{BV}(\mathbb{R}^d)$ has the ∞ -norm: in particular, λ is uniformly continuous. On the other hand, the evaluation map \mathbf{ev} is evaluation of persistence landscapes (which are piecewise linear functions) at a fixed set of points, so it is also 1-Lipschitz, hence uniformly continuous.

Claim 2: The discrete signature Σ is uniformly continuous. We need to prove that for any $\epsilon > 0$ there exists $\gamma > 0$ such that

$$\text{dist}_{\mathbf{TS}}(\underline{\mathbf{x}}, \underline{\mathbf{y}}) < \gamma \implies \|\Sigma^{\leq k}(\underline{\mathbf{x}}) - \Sigma^{\leq k}(\underline{\mathbf{y}})\|_{BW} < \epsilon .$$

From (3.15), and since we are working with a truncation of the discrete signature, it is enough to show the statement for any coefficient $|C_{\alpha_1, \dots, \alpha_\ell}^{\mathbf{x}} - C_{\alpha_1, \dots, \alpha_\ell}^{\mathbf{y}}|$.

Given $\underline{\mathbf{x}}, \underline{\mathbf{y}} \in \mathbf{TS}(\mathbb{R}^d)$ of length n , consider their difference time-series $\Delta \underline{\mathbf{x}}, \Delta \underline{\mathbf{y}}$ of length $n-1$. Flatten them in the vectors $\Delta \underline{\mathbf{x}} := (\Delta \mathbf{x}_1, \dots, \Delta \mathbf{x}_{n-1})$ and $\Delta \underline{\mathbf{y}} := (\Delta \mathbf{y}_1, \dots, \Delta \mathbf{y}_{n-1})$ of length $d(n-1)$. In the polynomial ring $\mathbb{R}[T_{11}, \dots, T_{1d}, T_{21}, \dots, T_{n-1d}]$ consider the polynomial

$$P(\mathbf{T}) := \sum_{1 \leq i_1 \leq \dots \leq i_\ell < n} p_1(T_{i_1 1}, \dots, T_{i_1 d}) \cdots p_\ell(T_{i_\ell 1}, \dots, T_{i_\ell d}) .$$

Then it holds

$$P(\Delta \underline{\mathbf{x}}) = \sum_{1 \leq i_1 \leq \dots \leq i_\ell < n} p_1(\Delta \mathbf{x}_{i_1}) \cdots p_\ell(\Delta \mathbf{x}_{i_\ell}) = C_{p_1 \otimes \dots \otimes p_\ell}^{\mathbf{x}} .$$

But polynomials (on a compact domain) are uniformly continuous, hence for any $\epsilon > 0$ there exists $\delta > 0$ such that

$$\|\Delta \underline{\mathbf{x}} - \Delta \underline{\mathbf{y}}\|_2 < \delta \implies |C_{p_1 \otimes \dots \otimes p_\ell}^{\mathbf{x}} - C_{p_1 \otimes \dots \otimes p_\ell}^{\mathbf{y}}| = |P(\Delta \underline{\mathbf{x}}) - P(\Delta \underline{\mathbf{y}})| < \epsilon .$$

Now, if

$$\text{dist}_{\mathbf{TS}}(\underline{\mathbf{x}}, \underline{\mathbf{y}}) := \max \{\|\mathbf{x}_i - \mathbf{y}_i\|_2 \mid i \in [n]\} \leq \frac{\delta}{2(n-1)} ,$$

one gets

$$\|\Delta \mathbf{x}_{i+1} - \Delta \mathbf{y}_{i+1}\|_2 = \|\mathbf{x}_{i+1} - \mathbf{x}_i - \mathbf{y}_{i+1} + \mathbf{y}_i\|_2 \leq \|\mathbf{x}_{i+1} - \mathbf{y}_{i+1}\|_2 + \|\mathbf{x}_i - \mathbf{y}_i\|_2 \leq \frac{\delta}{n-1}$$

implying that on the flattenings it holds

$$\|\Delta_{\mathbf{x}} - \Delta_{\mathbf{y}}\|_2 \leq \sum_{j \in [n-1]} \|\Delta \mathbf{x}_j - \Delta \mathbf{y}_j\|_2 \leq \delta.$$

We conclude that it is enough to take $\gamma := \frac{\delta}{2(n-1)}$ so that the hypothesis $\text{dist}_{\mathbf{TS}}(\underline{\mathbf{x}}, \underline{\mathbf{y}}) < \gamma$ implies $|C_{\alpha_1, \dots, \alpha_\ell}^{\mathbf{x}} - C_{\alpha_1, \dots, \alpha_\ell}^{\mathbf{y}}| < \epsilon$. This proves that the truncated discrete signature map is uniformly continuous. \square

We remark that discrete signatures characterise landscapes, hence barcodes, up to translating nonzero sections of a landscape along regions of the domain where the landscape is identically zero. Indeed, identically zero regions of the landscape produce consecutive zero vectors in the time-series of the critical points, and these can be contracted to a unique zero vector by time-warping.

4 Application to knotted proteins

In this section we apply discrete signatures on a dataset of knotted proteins that were analysed with persistence landscapes in [Ben+23].

The three-dimensional coordinates of the carbon (C-alpha) atoms of the protein (whose backbone forms an open-ended positive trefoil knot) form a point cloud, and serve as the input data for persistent homology. The proteins are categorised into structural classes based on amino-acid *sequence similarity* of the protein: proteins with sufficiently similar sequences of amino-acids are highly likely to have similar 3D structures. We adopt the same convention as [Ben+23] and label the class by a representative protein of the class, or “other” whenever there were insufficient similar sequences to define additional classes. The proteins were also labelled with a separate classification, either deeply or shallow knotted or “neither” when the protein was not classified as shallow or deeply knotted [Ben+23]. We refer the reader to [Ben+23] for more details.

In [Ben+23] the authors compute the persistence landscapes of these proteins and show that the L_1 -landscape and Wasserstein distances separate the proteins into nine structural classes labelled by representative (see legend in Figure 4.2).

Here, we used the software FRUITS (*Feature Extraction Using Iterated Sums*) [DK24] for implementation of the discrete signature of a time-series. The corresponding code for this section is publicly available at <https://github.com/dtolosav/discrete-sig-for-landscapes>. We opted for a straightforward implementation of the DLFM in this work. Note that both path signatures and discrete signatures are amenable to kernelization [KO16; LO23], which has the potential to significantly improve computational aspects while preserving desirable properties.

Correlation between discrete signature and sequence similarity. Using discrete signatures with Euclidean distance (i.e. Bombieri-Weyl distance), we implement an unsupervised approach, in the sense that we assume no information about structural class. We use k-means clustering for three parameters: truncation of levels in the landscapes, truncation by weight (as defined in (3.3)) of the discrete signatures, and number of clusters for k-means. We quantify the correlation between signature-based clusters and the labelling determined by structural class representative using the *Adjusted Rand Index* (ARI) and *Normalised Mutual Information* (NMI) (see Figure 4.1). Proteins in the dataset whose structural class were labelled “other” were not considered in this analysis.

Levels	Weight (\leq)	Clusters	ARI	NMI
15	3	9	0.950	0.869
10	2	7	0.868	0.748
10	2	5	0.746	0.705
10	2	6	0.731	0.683
5	3	8	0.586	0.528
15	2	9	0.539	0.738
5	3	9	0.497	0.869
10	2	8	0.468	0.634
10	2	9	0.455	0.634
10	2	15	0.370	0.635

Figure 4.1: Correlations (via ARI and NMI) between the signature-based clusters and the labeling determined by 9 structural class representative. The first row highlights a significantly high correlation after truncating the landscape at the first 15 levels, the discrete signature at weight 3 and imposing 9 clusters.

The metrics in Figure 4.1 show high similarity between the clustering based on the 9 structural class representatives, and the k-means clustering using the first 15 levels of landscapes, discrete signatures up to weight 3, and 9 clusters, with ARI of 0.958 and NMI of 0.895. We find it remarkable that such a high accuracy is already reached by truncating the discrete signature up to weight 3. We will work with these parameters in the remainder of the section.

The above ARI and NMI scores outperform the alternative k-means clustering algorithm that uses L_1 distance on the landscapes directly, which gives ARI 0.88 of and NMI of 0.83. Furthermore, the dimension of feature vectors produced by our (more descriptive) discrete signature method is significantly lower than the ones by directly using landscapes.

We can visualise the results of Figure 4.1 in Figure 4.2: the signature-based clustering separates all structural class representatives except 3ZNC (in orange – not dominant in any cluster) and 1FUG (in mauve – dominant in two clusters). However, these exceptions are acceptable and justified by some particular features of the protein dataset considered in [Ben+23]. Indeed, the protein class 3ZNC (orange) is broken, presenting missing parts in the amino-acids chain, and it has a similar structure chain to 4QEF (navy blue), as they are both carbamoyltransferases.

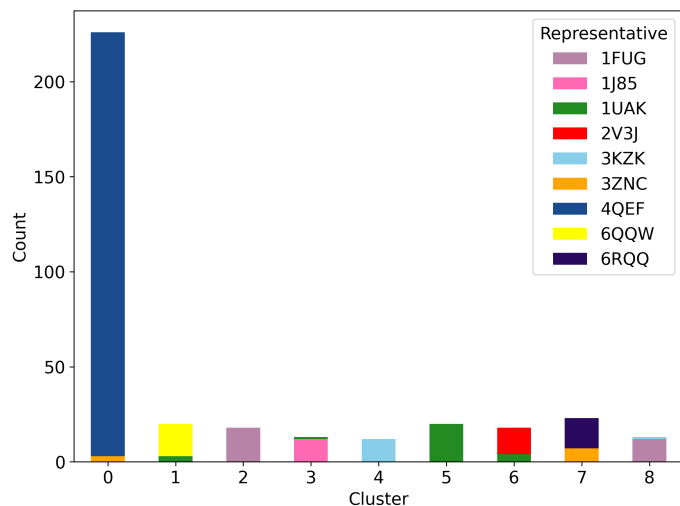


Figure 4.2: k-means clustering using 15 levels, weight ≤ 3 , and 9 clusters as parameters.

Validation of the correlation test. *A priori* the above high accuracy can just be a coincidence, in which case our test would be unreliable. Therefore, we also performed a permutation test (see Figure 4.3), and obtained p-values ≤ 0.001 for ARI and NMI, showing statistical significance of the scores obtained in Figure 4.1.

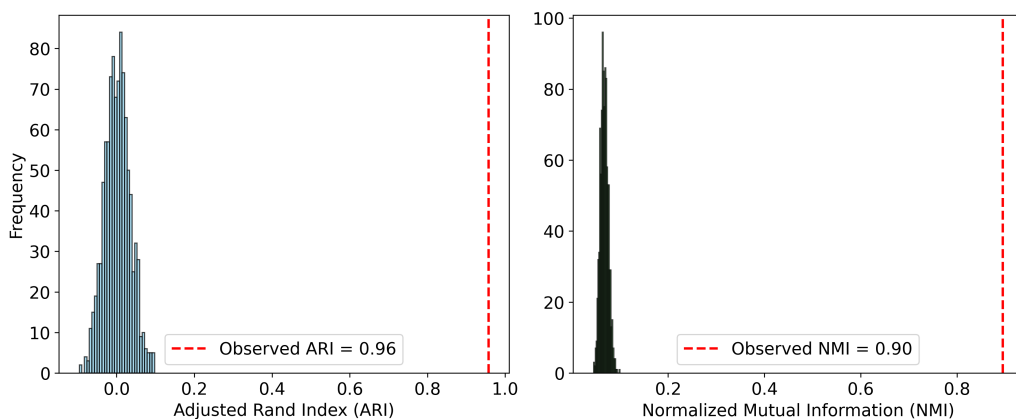


Figure 4.3: Permutation test for ARI and NMI (p-value 0.001), with parameters as in Figure 4.2.

The vertical bars in Figure 4.3 represent the score (ARI or NMI) obtained with random inputs, while the dashed red line represents the score observed by running the test with the chosen protein dataset. The fact that the score we obtain is far from the “random” scores validates our test as reliable for protein datasets.

We further investigate how well the discrete signature captures structural classes by running a *centroid-based permutation test with separation ratio*: we compute the *average signature* within each structural class, and we compute the *separation ratio*, i.e. between-class/within-class distances. This is analogous to the test used in [Ben+23] using average landscapes. We obtain a separation ratio of 2.49 with a p-value < 0.001 (cf. Figure 4.4). This test is independent of the k-means clustering.

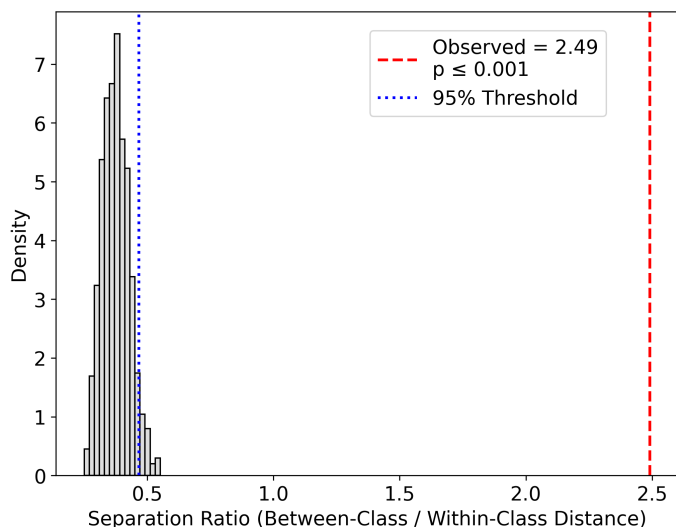


Figure 4.4: Centroid-based permutation test using separation ratio with average signatures.

A large ratio means that different classes have different discrete signatures; equivalently, signatures separate structural classes. Figure 4.4 shows that signatures do not separate random classes, for which the ratio is < 0.5 (dashed blue line), in contrast to the ratio of 2.49 (dashed red line) obtained with the protein dataset. Again, this test validates a strong correlation between discrete signatures and clustering of structural classes.

Correlation between discrete signature and knot depth. The previous analysis confirms that the discrete signature distinguishes structural representative classes. Now, we look into a different feature of interest, namely the *knot depth* (see [BG21] for a precise definition). Here, we consider the entire dataset, including proteins with structural class representative listed as “other”. We quantify the correlation between discrete signatures and knot depth via two standard methods. The **Spearman Correlation** method returns a depth-signature distance correlation of 0.647 with $p\text{-value} < 0.001$, showing correlation with statistical significance. The method **Random forest for predictive power** gives a R^2 score for depth prediction of 0.866 ± 0.048 . Here, values close to 1 indicate strong predictive performance, hence the model explains the 86.6% of the variance in knot depth using the discrete signature. Again, we refer to <https://github.com/dtolosav/discrete-sig-for-landscapes> for a more detailed analysis and code.

Signature-knot depth correlation via PCA. We visualise the signature-knot depth correlation via principal component analysis (PCA). Figure 4.5 is obtained by considering the first three principal components. Following [Ben+23], we label our proteins as *deep* whenever $depth > 0.05$, *shallow* whenever $depth < 0.005$, and *neither* for intermediate values. Be aware that the top plot (colored by representative classes) does not include the representative class labeled as “other”, while the bottom plot (colored by depth classes) does. The clusterings obtained

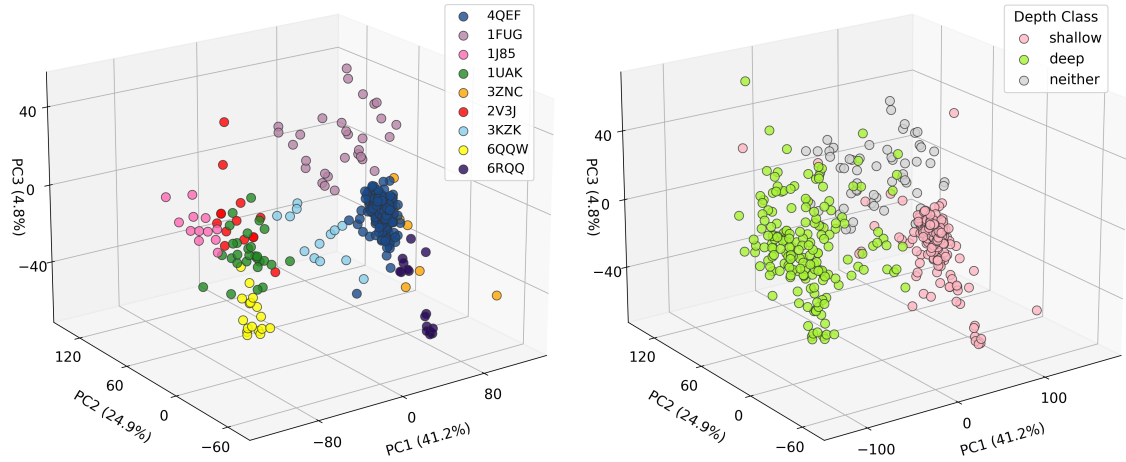


Figure 4.5: 3-dimensional PCA colored by structural class representative (left) and by knot depth classification (right).

via PCA in Figure 4.5 are finer than the ones obtained via ISOMAP in [Ben+23, Figure 2(b)]. Further visualisations, including some via ISOMAP, are available in <https://github.com/dtolosav/discrete-sig-for-landscapes>.

References

- [Ali+23] D. Ali, A. Asaad, M.J. Jimenez, V. Nanda, E. Paluzo-Hidalgo, and M. Soriano-Trigueros. “A survey of vectorization methods in topological data analysis”. In: *IEEE Transactions on Pattern Analysis and Machine Intelligence* 45.12 (2023), pp. 14069–14080.
- [AFS19] C. Améndola, P. Friz, and B. Sturmfels. “Varieties of signature tensors”. In: *Forum Math. Sigma* 7 (2019), Paper No. e10, 54. ISSN: 2050-5094. DOI: 10.1017/fms.2019.3.
- [Amé+25] C. Améndola, F. Galuppi, Á.D. Ríos Ortiz, P. Santarsiero, and T. Seynnaeve. “Decomposing Tensor Spaces via Path Signatures”. In: *Journal of Pure and Applied Algebra* 229.1 (2025). DOI: 10.1016/j.jpaa.2024.107807.
- [BG21] A. Barbensi and D. Goundaroulis. “f-distance of knotoids and protein structure”. In: *Proceedings of the Royal Society A* (2021). DOI: 10.1098/rspa.2020.0898.
- [BP23] C. Bellingeri and R. Penaguiao. “Discrete signature varieties”. In: *arXiv preprint arXiv:2303.13377* (2023).
- [Ben+23] K. Benjamin, L. Mukta, G. Moryoussef, C. Uren, H.A Harrington, U. Tillmann, and A. Barbensi. “Homology of homologous knotted proteins”. In: *Journal of the Royal Society Interface* 20.201 (2023), p. 20220727.

- [Ben+24] K. Benjamin et al. “Multiscale topology classifies cells in subcellular spatial transcriptomics”. In: *Nature* (2024), pp. 1–7.
- [Bub15] P. Bubenik. “Statistical topological data analysis using persistence landscapes.” In: *J. Mach. Learn. Res.* 16.1 (2015), pp. 77–102.
- [Bub20] P. Bubenik. “The Persistence Landscape and Some of Its Properties”. In: *Topological Data Analysis*. Springer International Publishing, 2020, pp. 97–117. ISBN: 9783030434083. DOI: 10.1007/978-3-030-43408-3_4.
- [BD17] P. Bubenik and P. Dlotko. “A persistence landscapes toolbox for topological statistics”. In: *Journal of Symbolic Computation* 78 (2017), pp. 91–114. DOI: 10.1016/j.jsc.2016.03.009.
- [Bub+20] P. Bubenik, M. Hull, D. Patel, and B. Whittle. “Persistent homology detects curvature”. In: *Inverse Problems* 36.2 (2020), p. 025008. DOI: 10.1088/1361-6420/ab4ac0.
- [Che54] K.T. Chen. “Iterated integrals and exponential homomorphisms”. In: *Proceedings of the London Mathematical Society* 3.1 (1954), pp. 502–512.
- [CNO20] I. Chevyrev, V. Nanda, and H. Oberhauser. “Persistence Paths and Signature Features in Topological Data Analysis”. In: *IEEE Transactions on Pattern Analysis and Machine Intelligence* 42.1 (Jan. 2020), pp. 192–202. DOI: 10.1109/tpami.2018.2885516.
- [CEH07] D. Cohen-Steiner, H. Edelsbrunner, and J. Harer. “Stability of persistence diagrams”. In: *Discrete Comput. Geom.* 37.1 (2007), pp. 103–120.
- [DET20a] J. Diehl, K. Ebrahimi-Fard, and N. Tapia. “Iterated-sums signature, quasi-symmetric functions and time series analysis”. In: *Sém. Lothar. Combin.* (2020). DOI: 10.34657/8424.
- [DET20b] J. Diehl, K. Ebrahimi-Fard, and N. Tapia. “Time-warping invariants of multidimensional time series”. In: *Acta Applicandae Mathematicae* 170.1 (2020), pp. 265–290. DOI: 10.1007/s10440-020-00333-x.
- [DET22] J. Diehl, K. Ebrahimi-Fard, and N. Tapia. “Tropical Time Series, Iterated-Sums Signatures, and Quasisymmetric Functions”. In: *SIAM Journal on Applied Algebra and Geometry* 6.4 (2022), pp. 563–599. DOI: 10.1137/20M1380041.
- [DK24] J. Diehl and R. Krieg. “FRUITS: feature extraction using iterated sums for time series classification”. In: *Data Min Knowl Disc* 38 (2024), pp. 4122–4156. DOI: 10.1007/s10618-024-01068-1.
- [FLS24] P. Friz, T. Lyons, and A. Seigal. “Rectifiable paths with polynomial log-signature are straight lines”. In: *Bulletin of the London Mathematical Society* 56.9 (2024), pp. 2922–2934.
- [GS24] F. Galuppi and P. Santarsiero. *Rank and symmetries of signature tensors*. 2024. arXiv: 2407.20405 [math.AG].
- [Gar+22] R.J Gardner, E. Hermansen, M. Pachitariu, Y. Burak, N. A Baas, B.A Dunn, M-B. Moser, and E.I Moser. “Toroidal topology of population activity in grid cells”. In: *Nature* 602.7895 (2022), pp. 123–128.

- [Giu+25] C. Giusti, D. Lee, V. Nanda, and H. Oberhauser. “A topological approach to mapping space signatures”. In: *Advances in Applied Mathematics* 163 (2025), p. 102787.
- [HL10] B. Hambly and T. Lyons. “Uniqueness for the signature of a path of bounded variation and the reduced path group”. In: *Annals of Mathematics* 171.1 (Mar. 2010), pp. 109–167. DOI: 10.4007/annals.2010.171.109.
- [KO16] F.J. Király and H. Oberhauser. *Kernels for sequentially ordered data*. arXiv:1601.08169 [stat]. Jan. 2016. DOI: 10.48550/arXiv.1601.08169.
- [LO23] D. Lee and H. Oberhauser. *The Signature Kernel*. arXiv:2305.04625 [math]. May 2023. DOI: 10.48550/arXiv.2305.04625.
- [Lee+17] Y. Lee, S.D Barthel, P. Dłotko, S.M. Moosavi, K. Hess, and B. Smit. “Quantifying similarity of pore-geometry in nanoporous materials”. In: *Nature communications* 8.1 (2017), pp. 1–8.
- [LM25] T. Lyons and A.D McLeod. *Signature Methods in Machine Learning*. 2025. arXiv: 2206.14674 [stat.ML].
- [Mil15] E. Miller. “Fruit flies and moduli: interactions between biology and mathematics”. In: *Notices of the AMS* 62.10 (2015), pp. 1178–1184.
- [Ott+17] N. Otter, M.A. Porter, U. Tillmann, P. Grindrod, and H.A. Harrington. “A roadmap for the computation of persistent homology”. In: *EPJ Data Science* 6.1 (2017), p. 17. DOI: 10.1140/epjds/s13688-017-0109-5.
- [RB19] R. Rabadán and A.J Blumberg. *Topological data analysis for genomics and evolution: topology in biology*. Cambridge University Press, 2019.

(V. Galgano) MAX-PLANCK INSTITUTE OF MOLECULAR CELL BIOLOGY AND GENETICS, DRESDEN, GERMANY; CENTRE FOR SYSTEMS BIOLOGY DRESDEN, DRESDEN, GERMANY; FACULTY OF MATHEMATICS, TECHNISCHE UNIVERSITÄT DRESDEN, DRESDEN, GERMANY; *E-mail address*: galgano@mpi-cbg.de; ORCID: 0000-0001-8778-575X

(H. A. Harrington) MAX-PLANCK INSTITUTE OF MOLECULAR CELL BIOLOGY AND GENETICS, DRESDEN, GERMANY; CENTRE FOR SYSTEMS BIOLOGY DRESDEN, DRESDEN, GERMANY; FACULTY OF MATHEMATICS AND PHYSICS OF LIFE, TECHNISCHE UNIVERSITÄT DRESDEN, DRESDEN, GERMANY; MATHEMATICAL INSTITUTE, UNIVERSITY OF OXFORD, OXFORD, UK; *E-mail address*: harrington@mpi-cbg.de; ORCID: 0000-0002-1705-7869

(D. Tolosa) SCHOOL OF MATHEMATICAL AND STATISTICAL SCIENCES, ARIZONA STATE UNIVERSITY, TEMPE, AZ, UNITED STATES OF AMERICA; *E-mail address*: dtolosav@asu.edu ; ORCID: 0000-0003-0586-9808